HYDROTHERMAL SYNTHESIS AND CHARACTERIZATION OF LIMNPO4 FOR SECONDARY LITHIUM BATTERIES

A THESIS SUBMITTED TO
THE GRADUATE SCHOOL OF NATURAL AND APPLIED SCIENCES
OF
MIDDLE EAST TECHNICAL UNIVERSITY

BY

ESİN CAMCI

IN PARTIAL FULFILLMENT OF THE REQUIREMENTS
FOR
THE DEGREE OF MASTER OF SCIENCE
IN
METALLURGICAL AND MATERIALS ENGINEERING

SEPTEMBER 2014

Approval of the thesis:

HYDROTHERMAL SYNTHESIS AND CHARACTERIZATION OF LIMNPO4 FOR SECONDARY LITHIUM BATTERIES

submitted by **ESİN CAMCI** in partial fulfillment of the requirements for the degree of **Master of Science in Metallurgical and Materials Engineering Department, Middle East Technical University** by,

Prof. Dr. Canan Özgen
Dean, Graduate School of **Natural and Applied Sciences** _____

Prof. Dr. C. Hakan Gür
Head of Department, **Metallurgical and Materials Engineering** _____

Prof. Dr. M. Kadri Aydınol
Supervisor, **Metallurgical and Materials Eng. Dept., METU** _____

Examining Committee Members:

Prof. Dr. Macit Özenbaş
Metallurgical and Materials Eng. Dept., METU _____

Prof. Dr. M. Kadri Aydınol
Metallurgical and Materials Eng. Dept., METU _____

Assoc. Prof. Dr. Caner Durucan
Metallurgical and Materials Eng. Dept., METU _____

Assoc. Prof. Dr. Emrah Ünalan
Metallurgical and Materials Eng. Dept., METU _____

Assoc. Prof. Dr. Zafer Evis
Engineering Sciences Dept., METU _____

Date: 01.09.2014

I hereby declare that all information in this document has been obtained and presented in accordance with academic rules and ethical conduct. I also declare that, as required by these rules and conduct, I have fully cited and referenced all material and results that are not original to this work.

Name, Last Name: Esin CAMCI
Signature:

ABSTRACT

HYDROTHERMAL SYNTHESIS AND CHARACTERIZATION OF LIMNPO4 FOR SECONDARY LITHIUM BATTERIES

Camcı, Esin

M. S., Department of Metallurgical and Materials Engineering

Supervisor: Prof. Dr. M. Kadri Aydınol

September 2014, 77 Pages

The mechanism in Li-ion batteries is based on the motion of Li^+ ion between positive and negative electrodes. As Li-ion batteries have attracted much attention, the demand for high capacity and low cost electrode materials has increased. Lithium manganese phosphate (LMnP) is one of the most promising cathode materials. It highly satisfies the lithiation and de-lithiation process of Li-ion technology due to its olivine structure. Moreover, it has high theoretical capacity, it is safety and low cost. The drawback of LMnP is its poor ionic and electronic conductivity. The aim of this thesis is to optimize the hydrothermal process parameters for the synthesis of pure and well-crystalline LMnP, dope the Mn-site in the olivine structure with cobalt, chromium, molybdenum, vanadium and tungsten and eventually electrochemically characterize the samples to analyze the effect of doping. The structure and topography of the obtained powders were investigated with X-Ray Diffraction and Scanning Electron Microscopy. Also, the electrochemical characteristics were

determined by different techniques; cycle tests, charge-discharge, Cyclic Voltammetry and Electrochemical Impedance Spectroscopy. According to the results, doping process was successful to show better performance than pristine LMnP. After pure LMnP and its doped versions were analyzed, it is understood that cobalt and vanadium enhances the electrical and ionic conductivity of LMnP; whereas, chromium has an influence on the rate capability of LMnP.

Keywords: Lithium Manganese Phosphate, Hydrothermal Synthesis, Doping, Electrical Conductivity, Electrochemical Performance, Structural Characterization.

ÖZ

İKİNCİL LİTYUM BATARYALAR İÇİN LIMNPO4 MALZEMESİNİN HİDROTERMAL SENTEZİ VE KARAKTERİZASYONU

Camcı, Esin

Yüksek Lisans, Metalurji ve Malzeme Mühendisliği Bölümü

Tez Yöneticisi: Prof. Dr. M. Kadri Aydınol

Eylül 2014, 77 Sayfa

Li-iyon bataryaların mekanizması Li^+ iyonunun pozitif ve negatif elektrotlar arasındaki hareketine dayanır. Li-iyon bataryalara olan ilgi arttıkça yüksek kapasiteli ve düşük maliyetli elektrot malzemelerine olan talep artmaktadır. Lityum mangan fosfat (LMnP) en çok gelecek vadeden katot malzemelerinden biridir. Bu bileşiğin olivin yapısı Li-iyon teknolojisindeki lithasyon ve delithasyon tepkimelerini yüksek seviyede sağlar. Ayrıca, bu malzeme yüksek teorik kapasite değerine ve güvenlik unsurlarına sahip olmakla birlikte düşük maliyetlidir. LMnP yapısının eksik olduğu noktalar ise düşük iyonik ve elektriksel iletkenliğe sahip olmasıdır. Bu tezin amacı, saf ve kristal yapıdaki LMnP bileşiğini üretmek için hydrothermal proses parametrelerini optimize etmek, yapıdaki Mn pozisyonlarını kobalt, krom, molibden, vanadyum ve tungsten ile alaşımlandırmak ve son olarak de alaşımlama etkisi

incelemek adına numunelerin elektrokimyasal karakterizasyonunu yapmaktır. Elde edilen numunelerin yapısal ve topografik incelemesi X-Işınları Difraksiyonu ve Taramalı Elektron Mikroskobu ile yapılmıştır. Ayrıca, elektrokimyasal karakterizasyon için çeşitli teknikler kullanılmıştır; çevrim testleri, şarj-deşarj, çevrimsel voltametri ve elektrokimyasal empedans spektroskopi. Sonuçlar doğrultusunda, alaşımlama işleminin başarılı olduğu ve alaşımlı numunelerin saf LMnP malzemesine gore daha iyi performans gösterdiği görülmüştür. Saf LMnP ve diğer numuneler analiz edildiğinde, Co ve V elementlerinin elektriksel ve iyonik iletkenliğii arttırdığı ve Cr elementinin şarj kabiliyeti üzerinde etkili olduğu görülmüştür.

Anahtar kelimeler: Lityum Mangan Fosfat, Hidrotermal Sentez, Doping, Elektriksel İletkenlik, Elektrokimyasal Performans, Yapısal Karakterizasyon.

Dedicated to my mom and dad …

ACKNOWLEDGEMENTS

It would not have been possible to write this master thesis without the guidance and help of the kind people around me, to only some of whom it is possible to give particular mention here.

Above all, I would like to express my deepest gratitude to my advisor, Prof. Dr. M. Kadri Aydınol for his guidance and support. His invaluable experience and knowledge have helped me create a better perspective not only on this thesis but also on life. It was my honor to study with him throughout the course of the studies.

I would like to express my warm thanks to my friends at the Metallurgical and Materials Engineering Department of METU, especially Dr. Atıl Büyükburç, Berke Pişkin, Burcu Kayıplar and Şafak Doğu. It would have been a lonely lab without them. Also, thanks to Önder Şahin and Serkan Yılmaz for their patience and support during XRD and SEM analysis.

Special thanks go to Tuba Demirtaş who was always willing to help and give her best suggestions. Her support during thesis writing was memorable.

I would like to express my deepest thanks to Pelin Korkut who is also experiencing such a challenging period in her life. It was very calming for me to talk to her during the rough times. I think we co- motivated each other. Also, thanks to Seda Türeç, Duygu Okutucu, Barış Elmacı and Duygu Tanrıverdi for their caring and encouragements. Although we all are apart from each other, they somehow helped me cheer up and continue.

I would also like to thank my parents for their endless support. They always stood by me with their best wishes.

Finally, I would like to thank my husband, Arda Bahadır Akça for his patience. Also, he provided the best atmosphere to write thesis and he was always there to motivate me. I believe it would not be possible to write this thesis without him.

TABLE OF CONTENTS

LIST OF TABLES

LIST OF FIGURES

CHAPTER 1

INTRODUCTION

1.1 The Development of Battery

In recent years, the technology has advanced dramatically and the utilization of batteries as power sources has become dominant. Batteries are used to unplug many different devices such as mobile phones, laptops, cameras and even electrical vehicles. Since the discovery of the battery in 1800 by Alessandro Volta, different types of batteries were developed according to the application area. Since 1900s, there have been a variety of batteries ranging from lead-acid accumulator to sodium-sulfur battery. As shown in Figure 1.1, the energy density of battery chemistries has increased dramatically throughout the years. Between 1950 and 2010, the energy density of secondary batteries increased by nearly 5 times, shown by the dashed line in Figure 1.1. If the trend of this increase does not change, the expectations for energy density by 2110 and 2177 are 500 $Wh \cdot kg^{-1}$ and 700 $Wh \cdot kg^{-1}$, respectively [1].

The increasing demand for energy dense batteries sparked research and development studies on new generation battery types and chemistries. Since 1990, Li-ion chemistry has accelerated the growth rate. The domination of Li-ion battery on energy density is seen by the solid line in Figure 1.1. The density value has nearly doubled itself in 20 years. The reason why Li-ion battery has attracted more attention

than other alternatives is its low cost, good electrochemical performance and lightweight.

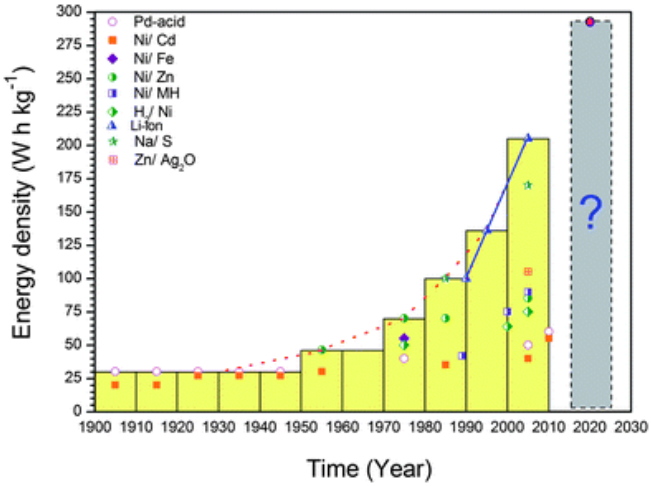

Figure 1.1. The development in the energy density of batteries in years [1].

1.2 Components of Batteries

A battery (chemical cell) converts chemical energy directly into electrical energy while it works. This conversion is favored by the oxidation and reduction reactions taking place inside the battery. The transfer of electrons from one substance to another through an electrical circuit is enabled by these reactions [2].

A battery involves one or more cells which are connected in series or parallel, or both. As indicated in Figure 1.2, each cell has four main components, which are anode, cathode, electrolyte and separator. There are many alternative materials to each one, so diverse combinations can be created. Among these combinations, materials having high voltage and capacity seem more efficient than the others; however, such combinations may not always be practical because of reactivity characteristics, high cost, difficulty in handling and polarization problems [2]. The components should be selected to be compatible with each other in terms of their chemistry and properties.

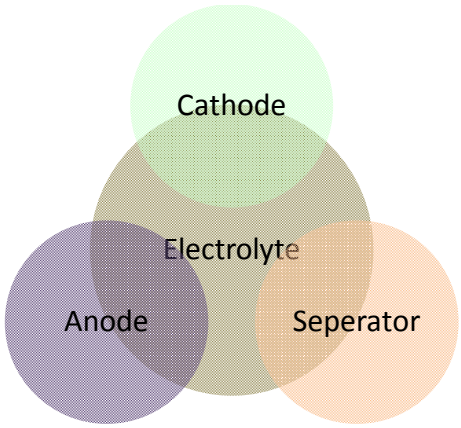

Figure 1.2. A chart illustrating the components of a cell.

Anode and cathode are the negative and positive electrodes, respectively. In anode side, oxidation reaction occurs and electrons flow out towards the external circuit during discharge [3]. On the other side, these electrons are attained and reduction of cathode material occurs. Both the anode and the cathode materials must have good conductivity and chemical stability in designed working voltage.

Electrolyte is the ionic conductor between anode and cathode. Usually being liquid, these conductors serve as the transfer medium for the motion of ions in the cell. Electrolyte must have high ionic conductivity to transfer the ions between electrodes. On the other hand, it must be electrically insulator because creating a contact between anode and cathode cause short circuit in the battery.

Separator is a porous material, which allows ionic transport but keeps the anode and cathode apart. It separates electrodes and avoids short circuit in the battery. Similar to electrolyte, the separator must be highly insulating and chemically stable to prevent decomposition.

Many alternative materials for each cell component exist. To illustrate them, the diversity of the battery designs increases the demand for different kinds of separator. Depending on the demand, many separator suppliers develop new generation materials and production techniques. For example, three different types of separator are seen Figure 1.3. They are made of polyethylene and polypropylene and manufactured with different deposition and stretching processes.

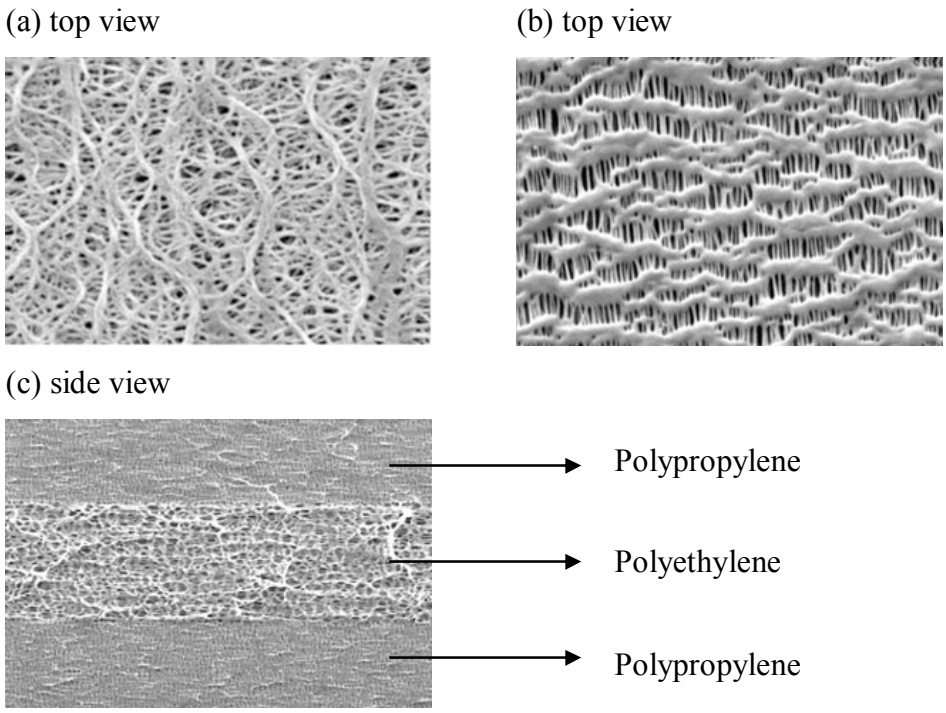

Figure 1.3. SEM images of Celgard (a) polyethylene, (b) polypropylene and (c) trilayer separators [2].

1.3 Classification of Batteries

Batteries can be classified according to their chemistry, operating principles or ability to be recharged. Classification of batteries considering their capability of being recharged is the most preferred method. In this manner, batteries can be classified as primary (non-rechargeable) and secondary (rechargeable) batteries. Typical primary and secondary batteries are given in Table 1.1.

Table 1.1. Examples to primary and secondary batteries with their voltage, capacity and specific energy [2].

Battery type	Anode	Cathode	Theoretical Values		
			Voltage (V)	Capacity (Ah/kg)	Specific Energy (Wh/kg)
Primary Batteries					
Silver oxide	Zn	Ag_2O	1.6	5.55	180
Li/FeS2	Li	FeS_2	1.8	1.38	726
Zinc/air	Zn	Ambient air	1.65	1.22	820
Magnesium	Mg	MnO_2	2.8	3.69	271
Secondary Batteries					
Lead-acid	Pb	PbO_2	2.05	8.32	120
Nickel-cadmium	Cd	Ni oxide	1.35	5.52	181
Silver-zinc	Zn	AgO	1.85	3.53	283

Primary batteries operate in such a way that the electrochemical reactions involved are non-reversible. This operation continues until the energy generating reactants are all consumed. In other words, the battery stops producing energy when the oxidation and reduction reactions of active materials are completed. Being light, easy to use and cheap, primary batteries are mostly used for remote controls, toys or any other portable devices. Even with these limited applications, primary batteries constitute 80% of the total batteries sold [4]. These types of batteries are commonly cylindrical or button shaped, excluding large batteries used in military applications and standby power systems, etc.

Secondary batteries can be used several times in contrast to primary ones. This reoperation ability is obtained by the use of different active reactants from the materials used in non-rechargeable batteries. After a secondary battery is discharged, it can be returned to its former state by the application of current in the opposite direction to discharge current. This process is called recharging. Having high power density and better discharge rate are characteristic features of secondary batteries. Advancements in technology promote the employment of secondary batteries, which are already at service for electronic devices, stationary systems and electrical vehicles.

1.4 Principles of Operation

The ionic motion and electron flow in a cell during discharge and charge are shown schematically in Figure 1.4. When the battery is connected to a device, electrons flow from anode to cathode. During this process, anode material is oxidized and cathode material is reduced. As the battery recharges, the flow of electrons is reversed and the electrodes where oxidation and reduction reactions take place change. In each operation, the circuit is completed with the motion of ions in the electrolyte.

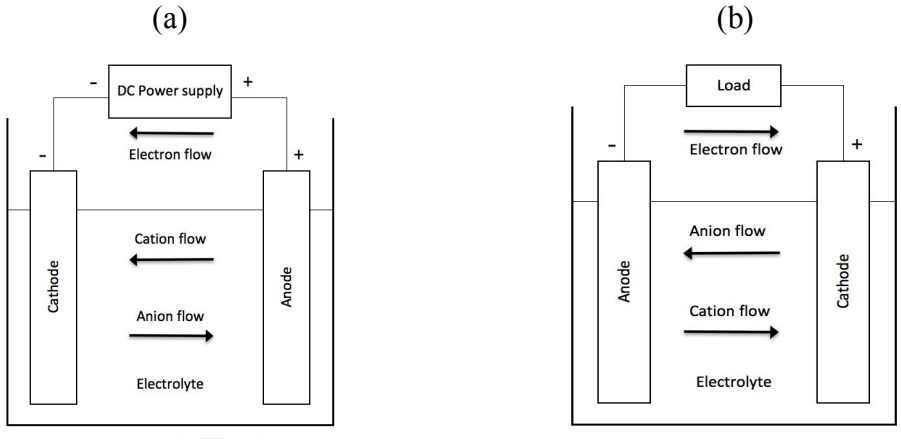

Figure 1.4. Schematics of (a) charge and (b) discharge of a cell [2].

To illustrate, the discharge-charge reactions taking place in positive and negative electrodes of lead-acid battery is given below. As indicated in Table 1.1, the lead-acid batteries have lead anode and lead dioxide cathode with sulfuric acid electrolyte. In lead-acid batteries, the electrolyte takes part in the processes together with the electrodes. The voltage for a lead-acid cell with 1.21 specific gravity electrolyte is 2.05 V [2]. While the cell discharges, both electrodes are converted to $PbSO_4$. Owing to being a secondary battery, the cell is recharged and the electrodes would return to their original chemistries by the reverse reactions. However, if it were a primary battery, it would be discarded when all the active materials are used with the completion of the discharge reactions.

Anode reaction

$$Pb + SO_4^{2-} \xrightarrow[\text{discharge}]{} PbSO_4 + 2e^- \qquad E_0 = 0.35\ V \qquad (1.1)$$

Cathode reaction

$$PbO_2 + SO_4^{2-} + 4H^+ + 2e^- \xrightarrow[\text{discharge}]{} PbSO_4 + 2H_2O \qquad E_0 = 1.70\ V \qquad (1.2)$$

Overall reaction

$$Pb + 2H_2SO_4 + PbO_2 \xrightarrow[\text{discharge}]{} 2PbSO_4 + 2H_2O \qquad E_{cell} = 2.05\ V \qquad (1.3)$$

CHAPTER 2

LI-ION BATTERIES

2.1 History of Lithium Batteries

Lithium batteries date back to 1970s. The early batteries were primary lithium batteries having metallic lithium negative electrodes. Because lithium is the lightest metal and has a high potential, Whittingham et al. proposed it being a good candidate for anode material [5].

Primary battery with lithium-sulfur dioxide chemistry was one of the first batteries which are commercially used. The first patent for this kind of cells was awarded in 1969 and they were commercially available by 1972 [3]. Afterwards, different cathode materials that have higher energy density and shelf life were developed and took place of lithium-sulfur dioxide batteries. Thionyl chloride, copper oxide, iron disulfide, silver chromate, manganese dioxide and carbon monofluoride were among such cathode materials [3]. Among these materials, manganese dioxide and carbon monofluoride have been still used in medical and industrial applications.

Since primary batteries with metallic lithium anode have safety problems, researchers aim to develop battery chemistries having different reaction mechanisms. Plus, lithium batteries have high energy density than other primary batteries, so

improving the properties of the existing structure and creating a rechargeable system were primary concerns [3]. As a consequence, Li-ion batteries were developed.

In 1979, Goodenough et al. demonstrated a secondary cell using $LiCoO_2$ (LCO) cathode and lithium metal anode [6]. LCO is a stable material that acts as a Li^+ ion donor. Having a Li^+ ion donor in cathode side eliminates the need for lithium metal anode. In other words, it enables to use a non-lithium negative electrode material.

Parallel to the cathode material, Yazami et al. studied on graphite as a new generation anode material [7]. In 1980, they demonstrated reversible intercalation of Li^+ ion into graphite. The graphite developed by them is currently the most commonly used negative active material.

The combination of these studies on anode and cathode resulted in the development of a rechargeable Li-ion battery, which does not include metallic lithium. The absence of metallic lithium dramatically improved the safety. The reaction mechanism of this rechargeable type is based on the motion of Li^+ ion between positive and negative electrodes.

In 1983 and 1997, Goodenough et al. made a demonstration on spinel [8] and olivine [9] cathode materials, respectively. Since then, these cathode materials are commercially used. Today Li-ion batteries are used in cell phones, tablets, laptop computers, digital cameras, power tools, electric bikes and military devices. Moreover, new applications areas such as electric vehicles are expected to take place in the market. The reason why Li-ion batteries are mostly preferred is that they offer many advantages compared to the other types. They have high specific energy, a low

self-discharge rate, long cycle life and a broad operation temperature range [2]. These features enable the use of different types of Li-ion batteries to meet the market demand.

2.2 Construction of a Li-ion Cell

According to the market demand, there are hundreds of cylindrical, prismatic and pouch type Li-ion battery manufacturers around the world. As new application fields for energy storage develop, the demand for all these types of batteries will increase, so does the number of battery manufacturers. Wound cells are generally used for applications requiring less than 5 Ah; whereas, stacked prismatic configurations are available for large format batteries. Although Li-ion batteries differ in size and shape, the basic principles of operation remain identical for all of them and thus, the production methods are very similar.

A schematic of a wound cylindrical cell is shown in Figure 2.1. As mentioned in Section 1.2, there are 4 pillars in a cell; anode, cathode, separator and electrolyte. The first step of a Li-ion cell production is the preparation of anode and cathode. The positive and negative active materials are coated on aluminum and copper current collector foils, respectively. The foils are 10 to 20 μm and the coatings are 100 to 150 μm thick on both sides [10]. For high power applications, the coatings must be as thin as possible, for example 50 μm on each side. The coated material contains not only electrochemically active materials; but also, conductive agent and binder material. The agent increases the electrical conductivity within the electrode, while binder keeps the particles together. There are many different kinds of binder materials, which are polymer and water based. Polyvinylidene difluoride (PVDF) is one of the most popular polymer based binders; whereas, styrene-butadiene rubber (SBR) binder is widely preferred for water based usage.

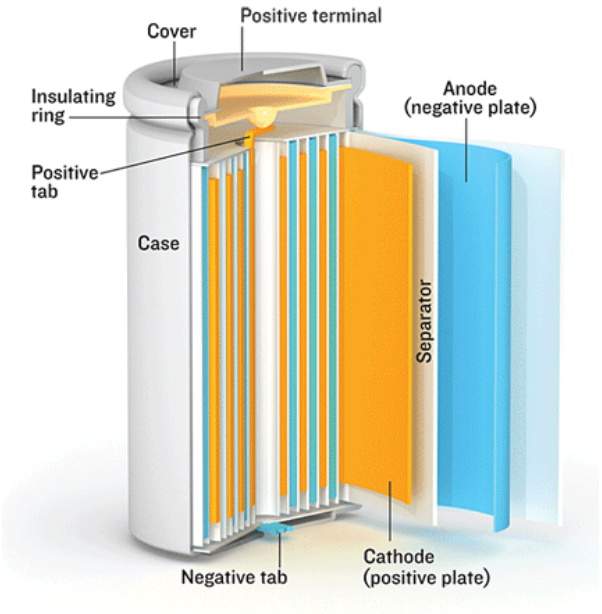

Figure 2.1. Schematic of a wound cylindrical Li-ion cells.

After electrode preparation, they are assembled with a 16 to 25 µm micro porous separator. As seen in Figure 2.1, in wound cells, the separator lies between the positive and negative electrodes to prevent the electrical contact. Besides, a specified welding process integrates positive and negative terminals. Lastly, the assembled unit is placed into a can or pouch with desired dimensions and filled with electrolyte. There are liquid, gel-polymer and solid electrolytes, which are commercially used. The electrolyte is selected depending on the active materials used. Despite the differences, the major mission of each electrolyte is providing a medium for Li^+ movement. Non-aqueous types are the most widely used electrolytes for Li-ion batteries.

2.3 Basic Concepts of Li-ion Batteries

The mechanism of Li-ion battery is based on the motion of Li^+ ions between positive and negative electrodes. As the battery is charged and discharged, Li^+ ions are inserted and extracted from the anode and cathode. This is literately called “rocking

chair" principle. Generally, in Li-ion batteries, lithium metal oxide or lithium metal phosphate are positive active materials and graphite is the negative active material. The motion of Li^+ ions and electrons during charging and discharging are graphically illustrated in Figure 2.2 and the related equations are as follows [2].

Positive $$LiMO_2 \xrightarrow[\text{discharge}]{} Li_{1-x}MO_2 + xLi^+ + xe^- \quad (2.1)$$

Negative $$C + xLi^+ + xe^- \xrightarrow[\text{discharge}]{} Li_xC \quad (2.2)$$

Cell $$LiMO_2 + C \xrightarrow[\text{discharge}]{} Li_{1-x}MO_2 + Li_xC \quad (2.3)$$

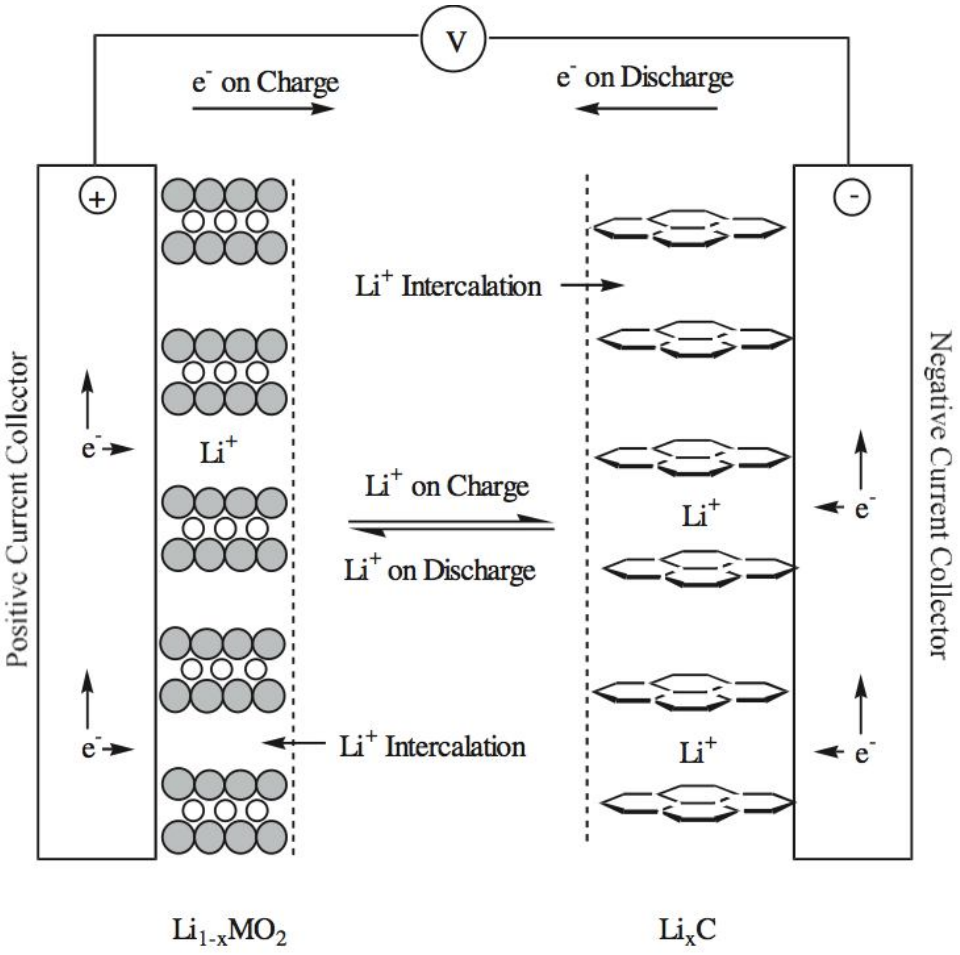

Figure 2.2. Schematic of the intercalation process in a Li-ion cell [2].

2.4 Positive Electrode Materials

For decades, the researchers have been studying on a variety of different cathode materials. There is a list prepared by Whittingham stating the criteria to be a good cathode material for Li-ion battery [11]. Analyses show that candidates that mostly satisfy the requisites are easily adapted to the commercial applications. Below is the Whittingham's list of requirements.

1. The material contains a readily reducible ion, for example a transition metal.
2. The material quickly reacts with lithium in a reversible manner.
   (a) This dictates an intercalation reaction in which the host structure essentially does not change as lithium is added.
3. The material reacts with lithium with a high free energy of reaction.
   (a) High capacity, preferably at least one lithium per transition metal.
   (b) High voltage, preferably around 4V (as limited by stability of electrolyte).
   (c) This leads to high energy storage.
4. The material reacts with lithium very rapidly both on insertion and removal.
5. The material be a good electronic conductor, preferably a metal.
   (a) This allows for the easy addition or removal of electrons during the electrochemical reaction.
   (b) This allows for reaction at all contact points between the cathode active material and the electrolyte rather than at ternary contact points between the cathode active materials and the electronic conductor.
   (c) This minimizes the need for inactive conductive diluents, which take away from the overall energy density.
6. The structure of the material is not affected and changed in over discharged and over charged state.
7. The material is low cost.
8. The material is environmentally safe [11].

The developed positive active materials generally have layered, spinel or olivine structures which are presented in Figure 2.3. Layered and spinel structured materials are lithium containing metal oxides and their derivatives, while olivine structured materials are lithium containing metal phosphates.

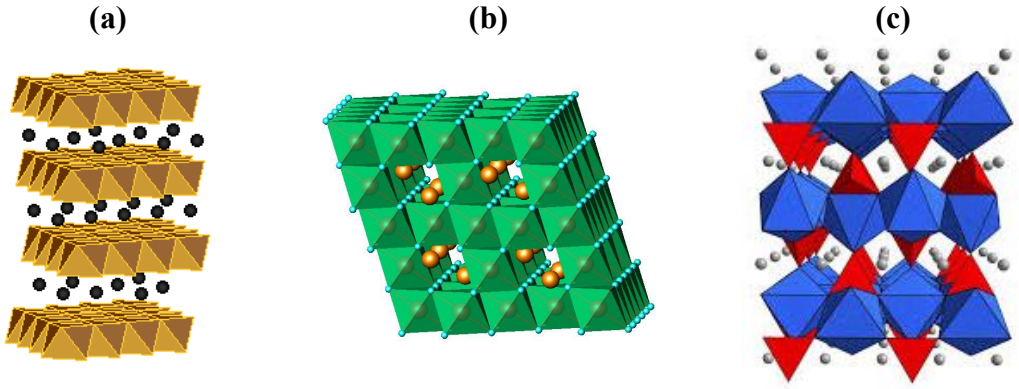

Figure 2.3 (a) Layered, (b) spinel and (c) olivine structures.

Each one of the abovementioned materials has its own characteristic crystal structure that directly relates to the Li^+ ion motion kinetics and other reaction mechanisms. In Table 2.1, the capacity and voltage values of different materials are provided.

Table 2.1 Voltage and capacity values of some positive active materials [2].

Material	Specific capacity (mAh/g)	Voltage vs. Li^0 at C/20 (V)
$LiCoO_2$ (LCO)	155	3.9
$LiNi_{1-x-y}Mn_xCo_yO_2$ (NMC)	140-180	≈ 3.8
$LiNi_{0.8}Co_{0.15}Al_{0.05}O_2$ (NCA)	200	3.73
$LiMn_2O_4$ (LMO)	100-120	4.05
$LiFePO_4$ (LFeP)	160	3.45
$LiMnPO_4$ (LMnP)	170	4.1

LCO has commercially been used as cathode active material for Li-ion batteries. Because preparation of LCO is very easy and simple, there has been much research on this material [2]. As seen from the charge-discharge curve of LCO in Figure 2.4, the working potential is about 3.9 V. The discharge capacity is about 155 mAh/g. However, LCO is tried to be replaced with other alternatives due to its high toxicity and cost.

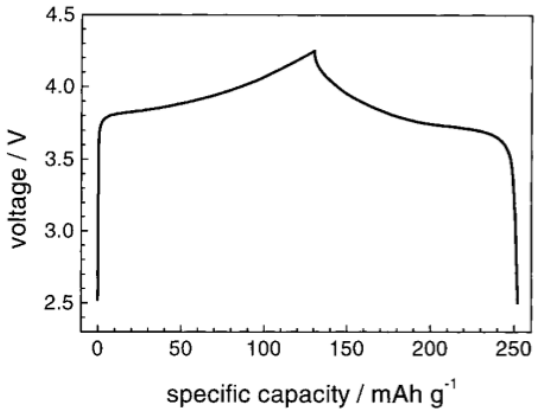

Figure 2.4. Typical charge- discharge characteristics of LCO.

$LiNi_{1-x-y}Mn_xCo_yO_2$ (NMC) and $LiNi_{0.8}Co_{0.15}Al_{0.05}O_2$ (NCA) are alternatives to LCO. They have the same crystal structure as LCO; therefore, they offer similar performance. They are advantageous since they are less expensive and have improved thermal stability to that of LCO [2]. Also, NCA materials have higher capacity at slightly lower voltage than LCO.

LMO has a spinel structure with the space group $Fd\bar{3}m$. This material is advantageous because it is highly available from natural sources and cost effective. Figure 2.5 shows the discharge characteristics of LMO [12]. It has two different discharge plateaus. Secondary batteries with LMO active material are generally designed to be used in high voltage plateau around 4 V. Because the operation voltage is high, an electrolyte that is resistant to oxidation is required [13]. Moreover,

LMO has very poor performance at high temperatures since it is very unstable. The basis of this instability is dissolution of Mn in electrolyte solution [14]. High temperature also affects the cycle life and storage performance of LMnO and causes it to quickly lose capacity. Although this material is mostly used in high voltage applications, it has the lowest capacity among other oxides. [15].

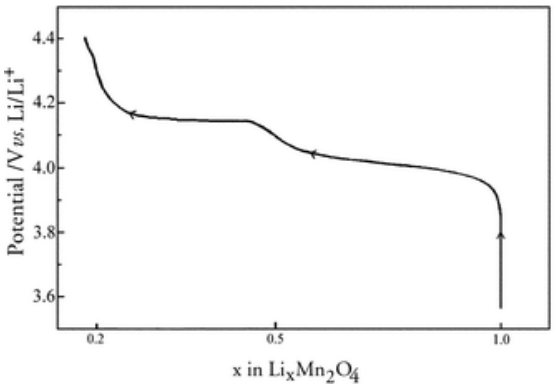

Figure 2.5. Discharge characteristic of LMnO [12].

LFeP and LMnP are phospho-olivines that suffer from low electrical and ionic conductivity. Because they contain iron and manganese rather than cobalt and can be found in nature as a mineral, these phospho-olivines are believed to be cheaper and more stable than LCO.

As seen in Table 2.1, LFeP has 160 mAh/g capacity and an average voltage of 3.45 V; whereas, LMnP has 4.1 V with 170 mAh/g theoretical capacity. In order to understand the characteristics and to achieve the theoretical performance of olivine materials, different studies were conducted. Another advantage of olivine materials is being benign and unreactive with other components in a cell.

In this thesis, LMnP was synthesized with hydrothermal method and the processing parameters were studied to improve the electrochemical performance of LMnP. Also, LMnP was doped with Co, Cr, Mo, V and W elements to replace Mn site. To our knowledge, these substitutional cations were not studied to improve the performance of LMnP cathode material.

CHAPTER 3

SYNTHESIS AND CHARACTERIZATION OF LMNP

3.1 Characteristic Features of LMnP

The three-dimensional framework of an olivine structure is stabilized by the strong covalent bonds between M – O and P – O resulting in polyanions [9]. As shown in Figure 3.1, the strong covalent bonds form a stable skeleton and create tunnels for Li^+ ion motion [16]. This eliminates atomic re-arrangements during Li^+ ion intercalation reactions and thus no capacity fade occurs after several cycles. The ordered olivine supports the motion of Li^+ ion along 1D tunnels in the structure. This provides fast kinetics during charging and discharging. Nevertheless, any atom rather than lithium that placed Li-site blocks the motion of Li^+ ion like a barrier in tunnel.

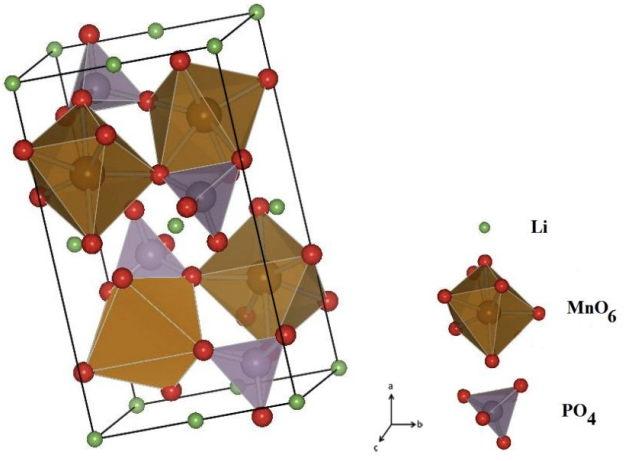

Figure 3.1. The structure of LMnP (Pnma) [16].

LMnP exhibits a potential plateau around 4.1 V vs. Li/Li^+ [9]. When high energy density is combined with being benign and low cost, LMnP becomes an attractive cathode material for Li-ion batteries. However, LMnP suffer from low electrical and ionic conductivity. These features are not desired for a cathode active material because they cause a poor discharge rate capability and electrochemical performance at high current densities. The reason of the low performance is slow diffusion kinetics within the material [17]. There are three main approaches to overcome the conductivity problem of LMnP; minimizing particle size [18], coating the particles with conductive carbon layer [19, 20] and finally doping LMnP structure with different elements [21, 22]. All of the actions against low conductivity aim to ease Li^+ ion motion and reduce the diffusion path of Li^+ ion in cathode active material [23].

3.2 Synthesis and Characterization of LMnP

There are many alternative methods like hydrothermal, sol-gel, co-precipitation and microwave assisted synthesis to produce olivine-type cathode active materials. According to Matsuda and Taniguchi, the crystallinity of cathode active materials strongly affects the electrochemical performance [24]. Hydrothermal synthesis is a wet chemical process which allows the synthesis of ordered and highly crystalline powder with a narrow particle size distribution. However, the synthesis parameters must be optimized and the boundary conditions must be well determined.

Delacourt et al. [25] produced LMnP particles with 100 nm diameter by co-precipitation. In their previous works, they obtained 35 mAh/g capacity from nearly 1 μm diameter particles and they enhanced the capacity to 70 mAh/g at a rate of 0.05 C. Yonemura et al. decreased the particle size of LMnP nearly to nano scale and reached to 150 mAh/g at 0.01 C, which is very close to theoretical value in Table 2.1. These studies prove that particle size is very critical in determining the capacity of the cathode material.

Chen et al. [26] state that hydrothermal synthesis is a powerful process when the key parameters are understood. They investigated the effects of temperature, reducing agents and additives.

There are different methods for carbon coating such as in-situ technique, sol-gel route and ball-milling. Murugan et al. [20] added a carbon source to hydrothermal medium and calcined the as-produced powder. According to their results, the carbon source was well dispersed and the particles were uniformly coated. However, the additional heat treatment increased the particle size. Yang et al. [19] preferred sol-gel method, which is not easy to control and needs a long time for aging the gel. Similar to Murugan et al., they needed further heating after powder production and obtained bigger particles. On the other hand, Moon et al. [27] used high-energy milling to coat LMnP produced by polyol process. They have seen that well-coated LMnP gave 49 – 52 mAh/g capacity at 0.1 C rate.

3.3 Doping of LMnP

As seen in Figure 3.1, LMnP has an orthorhombic structure consisting of close-packed phosphate anions with Mn^{2+} ions in corner sharing MnO_6 sites. There are many studies showing the improved performance of LMnP by Mn-site doping. Doping Mn-site with substitutional elements such as transition metal ions enhance the electrochemical performance of the parent phase [28]. Also, it is reported that high levels of doping are not soluble in the structure; but, form precipitates in the host.

Lee et al. synthesized cation substituted $LM_xMn_{1-x}P$, where M is Mg, Ca and Zr, by a solid-state reaction route and studied charge-discharge characteristics of LMnP. The phase analysis showed that doping level is a critical issue. LMnP structure can host the substitutional element to some extent; otherwise, different compounds of alloying

elements are formed. Also, they indicated that Mg and Zr doping improved the reversibility of the capacity and reduced polarization; however, Ca substitution deteriorates the performance. Upon the first charge-discharge cycle, the irreversible capacity loss was measured [21].

Dong et al. synthesized doped LMnP samples and focused on the effect of substitutional doping on the structure. They synthesized $LMg_{0.05}Mn_{0.05}P$ samples and characterized the structure with XRD. The obtained data was then refined with Rietveld Method. The diffraction pattern and the refinement results showed that doping does not change the crystal structure of LMnP and the dopant occupies the Mn site.

Chen et al. reported the negative effect of Zn substitution on the performance of LMnP. They also pointed out that there was some unidentified impurity present in their samples and it might influence the activity of the material [29].

CHAPTER 4

EXPERIMENTAL STUDIES

4.1 Synthesis of LMnP Powder

In this study, LMnP was synthesized by hydrothermal method. Hydrothermal system has various parameters, that control the reaction kinetics. All parameters affecting the formation and growth mechanism of LMnP particles were investigated in detail. Also, chelating agents, surfactants, reducing agents were used in hydrothermal media so as to manipulate the LMnP formation and decrease its particle size. In addition, doping Mn-site in LMnP structure with metal cations was studied to achieve better electrochemical characteristics of LMnP.

The precursors, as tabulated and provided in Table 4.1, were lithium hydroxide as Li source, manganese (II) acetate tetra hydrate as Mn source, and either ammonium phosphate or orthophosphoric acid as PO_4 source. Note that, since PO_4 source directly affects the pH of the reaction media, two separate experiments were conducted for each condition until it is fixed.

To begin with, the stoichiometric amounts of precursors were dissolved in distilled water. The solution was transferred into a Teflon-lined stainless steel autoclave which has an inner volume of 2 liters and heated to desired temperatures. Then, it was cooled down to room temperature. After hydrothermal reaction, the solution was

filtered and centrifuged to get white-pink precipitates. Following a typical synthesis, the precipitates were rinsed several times with distilled water and dried at 80 °C.

Table 4.1. The information about the precursor materials used to synthesis LMnP.

Source	Chemical Formula	Abbreviation	Company	Formula Weight (g/mol)
Li source	LiOH	LiH	Merck	23.95
Mn source	$Mn(CH_3COO)_2 \cdot 4H_2O$	MnAT	Aldrich	245.09
PO_4 source	$(NH_4)_3PO_4$	AmPh	Merck	115.02
	H_3PO_4	PhAc	Merck	97.99

In this thesis, the effects of concentration, molar ratio, temperature, time and pH were studied separately. That is, different values of them were tried while the others were kept constant. Also, the set of experiments and related values of parameters are as described below.

4.1.1 Effect of Concentration and Molar Ratio

Starting solution including higher precursor concentrations create more driving force for nucleation and increase the nucleation rate. Consequently, experiments were conducted with solutions having 0.15, 0.3 and 0.45 M Mn source with $Li/Mn/PO_4$= 3/1/1. Moreover, the concentrations of the precursors are adjusted according to the Mn^{2+} amount and molar ratio. As shown in Table 4.2, all the parameters except concentration and PO_4 source were kept constant.

To illustrate, in experiment no 1, 0.45 M LiH, 0.15 M MnAT and 0.15 M AmPh solutions (with molar ratio $Li/Mn/PO_4$= 3/1/1) were prepared and then mixed. The resulting solution was placed in the hydrothermal reactor and heated up to 200 °C.

Table 4.2. The set of experiments related to precursor concentration.

Exp No.	Li source	Mn source	PO_4 source	Molar Ratio ($Li/Mn/PO_4$)	Mn Concentration (M)	Temperature (°C)
1	LiH	MnAT	AmPh	3/1/1	0.15	200
2	LiH	MnAT	PhAc	3/1/1	0.15	200
3	LiH	MnAT	AmPh	3/1/1	0.3	200
4	LiH	MnAT	PhAc	3/1/1	0.3	200
5	LiH	MnAT	AmPh	3/1/1	0.45	200
6	LiH	MnAT	PhAc	3/1/1	0.45	200

The starting solutions having $Li/Mn/PO_4$ molar ratio of 3/1/1, 3/2/1 and 1.2/1/1 were prepared and hydrothermally reacted at 200 °C for 480 min. The reason why excess amount of LH was used is to create an alkaline medium, which is favorable for $LiMnPO_4$ formation. Following the analysis of obtained powders, it was seen that an optimization of molar ratio was also needed due to the formation of some undesired phases. The experiments numbered from 7 to 12 in Table 4.3 were conducted to find a reasonable ratio for precursors.

Table 4.3. The set of experiments related to molar ratio.

Exp No.	Li source	Mn source	PO_4 source	Molar Ratio ($Li/Mn/PO_4$)	Temperature (°C)	Time (min)
7	LiH	MnAT	AmPh	3/1/1	200	480
8	LiH	MnAT	PhAc	3/1/1	200	480
9	LiH	MnAT	AmPh	3/2/1	200	480
10	LiH	MnAT	PhAc	3/2/1	200	480
11	LiH	MnAT	AmPh	1.2/1/1	200	480
12	LiH	MnAT	PhAc	1.2/1/1	200	480

4.1.2 Effect of pH

pH, the measure of H^+ concentration in the reaction medium, is an important parameter for the formation of olivine-structured materials. For the formation of LMnP, an alkaline reaction medium is vital [25]. For this reason, different pH values were investigated, controlled by the addition of acidic and basic solutions, set of pH experiments were summarized in Table 4.4. The pH of the medium was monitored by a pH-meter (Sartorius PP-20).

Table 4.4. The set of experiments related pH.

Exp No.	Li source	Mn source	PO_4 source	Molar Ratio ($Li/Mn/PO_4$)	pH	Time (min)
13	LiH	MnAT	AmPh	1.2/1/1	<10	480
14	LiH	MnAT	AmPh	1.2/1/1	≈ 10	480
15	LiH	MnAT	AmPh	1.2/1/1	>10	480

4.1.3 Effect of Time

Time is one of the major parameters for a chemical reaction. In hydrothermal method, the dissolved ions in the precursor solution collide randomly and form different compounds. As time passes, many compounds form and then decompose. So as to understand the kinetics of LMnP system, the precursors under the same conditions were reacted at 200 °C for 240, 480 and 600 min, Table 4.5.

Table 4.5. The set of experiments related to reaction time.

Exp No.	Li source	Mn source	PO_4 source	Molar Ratio (Li/Mn/PO_4)	pH	Time (min)
16	LiH	MnAT	AmPh	1.2/1/1	10	240
17	LiH	MnAT	AmPh	1.2/1/1	10	480
18	LiH	MnAT	AmPh	1.2/1/1	10	600

4.1.4 Effect of Temperature

In all types of chemical reactions, increasing temperature creates more atomic vibrations and collisions, which result in an increase in the reaction rate. Different reaction temperatures of 120, 150 and 200 °C were studied to learn more about the reaction sequence of the precursors and to find the critical formation temperature of LMnP, set of temperature experiments were summarized in Table 4.6.

Table 4.6. The set of experiments related to temperature.

Exp No.	Li source	Mn source	PO_4 source	Molar Ratio (Li/Mn/PO_4)	Temperature (°C)	Time (min)
19	LiH	MnAT	AmPh	1.2/1/1	120	240
20	LiH	MnAT	AmPh	1.2/1/1	150	240
21	LiH	MnAT	AmPh	1.2/1/1	200	240

4.1.5 Effect of Additives

In an aqueous media, the presence of any kind of agent affects the reaction kinetics. In this study, different additives such as surfactants, reducing and chelating agents were used. Once standard procedure for the production of pure LMnP is optimized, the effect of the additives (as shown in Table 4.7) was studied. These agents were added to the starting solution while the precursors were mixed. Afterwards, it was expected that the agents affect the reaction mechanism and/or nucleation and growth kinetics of the LMnP formation.

Table 4.7. Technical details of the surfactants, chelating and reducing agents.

Additive Name	**Chemical Formula**	**Abbreviation**	**Producer Company**
D-(+)-Glucose anhydrous	$C_6H_{12}O_6$	GLU	Fluka
Citric acid monohydrate	$C_6H_8O_7 \cdot H_2O$	CA	Merck
Ethylene glycol	$HOCH_2CH_2OH$	EG	Alfa Aesar
(1-Hexadecyl) trimethyl-ammonium bromide	$CH_3(CH_2)_{15}N(CH_3)_3Br$	CTAB	Alfa Aesar
Sodium dodecyl sulfate	$C_{12}H_{25}NaO_4S$	SDS	Merck
Polyethylene glycol 400	$H(OCH_2CH_2)_nOH$	PEG	Alfa Aesar
Polyvinyl alcohol, low molecular weight	$[-CH_2CH(OH)-]_n$	PVA	Alfa Aesar
Igepal CO-890	$(C_2H_4O)_{40}C_{15}H_{24}O$	IGE	Sigma-Aldrich
Gelatin, Type B	-	GEL	Sigma
L-(+)-Ascorbic acid	$C_6H_8O_6$	LA	Alfa Aesar

4.2 The Effect Doping LMnP with Substitutional Elements

The doped LMnP powders with a chemical formula $LiMn_{0.95}M_{0.05}PO_4$ (LMnMP) where M is Co, Cr, Mo, V and W were synthesized with the optimized parameters. The starting chemicals and dopant precursors are tabulated and provided in Table 4.8.

The starting solution was prepared with the molar ratio of Li/Mn/M/PO4= 1.2/0.95/0.05/1 because doping Mn-sites with 5% is aimed. Similar to the procedure of pure LMnP synthesis, the solution including dopant source was prepared. Then, it was heated up to 200 °C and kept at that temperature for 240 min. The precipitates were filtered and washed with deionized water. The obtained samples were characterized in terms of structure and electrochemical performance.

Table 4.8. The starting precursors of doping experiments.

Sample Name	Alloying Element (M)	Li source	Mn source	PO_4 source	Dopant Source	Formula Weight (g/mol)
HT-V5	V	LH	MnAc	AmPh	Ammonium Vanadium Oxide	116.98
HT-Cr5	Cr	LH	MnAc	AmPh	Ammonium Chromate	152.07
HT-Co5	Co	LH	MnAc	AmPh	Cobalt Acetate Tetrahydrate	249.08
HT-Mo5	Mo	LH	MnAc	AmPh	Ammonium Heptamolybdate Tetrahydrate	1235.86
HT-W5	W	LH	MnAc	AmPh	Ammonium Tungsten Oxide Hydrate	2938.41

4.3 Structural Characterization

X-Ray diffraction was performed on a Rigaku DMAX 2200 using Cu Kα radiation (λ= 1.54056 Å). The diffraction data was collected from 10° to 80° (2θ) at a scan speed of 2 degree per minute. Rietveld method was used to refine the X-Ray datasets and to characterize the phase structures. By using MAUD program, quantitative phase analysis and structural refinements (lattice parameters, atomic positions and occupancy) were achieved. For doped samples, site occupation was investigated by Rietveld analysis to find out the replacement of dopant with Mn atom.

The particle morphology and surface topography were investigated by FEI Nova Nano 430 Field Emission Scanning Electron Microscopy (FE-SEM) at an operating voltage of 20 V. Moreover, qualitative analyses were done with an Energy Dispersive X-Ray Spectroscopy (EDX). For SEM analysis, powder samples were anchored onto aluminum studs through carbon tape. Since synthesized powders are not conductive, samples were coated with 10 nm gold. Images were recorded at minimum 10 kV with secondary electrons mode.

The particle size distribution is examined by Mastersizer 2000. The refractive index was set as default and distilled water was used as dispersant during all measurements. Also, different levels of ultrasound were used to refine the agglomerated powder.

4.4 Electrical Measurements

4.4.1 Pellet Preparation and Sintering

In order to make the electrical measurements, the synthesized pristine samples were first pelletized and then sintered to get the desired shape. Pressing is a process to

form powder materials with various morphologies into a particular shape. To serve this purpose, many lubricants, binders and additive materials can be used. Lubricants eliminate the frictional forces between particles and die; whereas, binders play an important role in the interaction of particles.

For the best pellet quality, the optimum pressing conditions were studied. Also, the conventional die apparatus was modified with springs to have a double-sided pressing. As a result, 0.5 g pristine LMnP powder were pressed into a 12 mm diameter pellet by a hydraulic press at 6.9 Bar (100 Psi) and kept at that pressure for 20 s. No binder material was used, only the die walls were lubricated by stearic acid. Notice that the measured values would not be accurate if the sample contains any phase or defect rather than LMnP.

Following pressing, pellets were sintered at 950 °C for 2 h. The effect of different sintering atmospheres was studied and it was found that pellets should be prepared under vacuum rather than inert atmosphere or open-air performed best. During sintering proses, the vacuum was below 10^{-5} mbar. The sintered pellets were carefully grinded and fine polished until the two surfaces of the pellet were parallel and smooth. Subsequently, silver paste is painted on both faces of the pellet so as to ensure the conductive contact area.

4.4.2 Electrical Conductivity Test

Electrical conductivity is the ability of a material to carry electrical current. The electrical conductivity of LMnP samples was measured by DC current-voltage method. These measurements were made using Solartron MTS test system. DC conductivity measurements were made by scanning the potential between 20 and 80 V with 100 mV/sec scan rate. The slope of the I-V curve gives the DC conductivity of the material.

4.5 Carbon Coating

The powders synthesized with hydrothermal method needs a secondary carbon coating process because a continuous carbon layer on the particles plays a significant role in electrical conductivity. LMnP can be coated by either pyrolyzing at 600 °C with a carbon source such as sucrose or mechanically coating in a ball-mill with carbon black.

In pyrolysis process, as-produced powders were mixed with sucrose in an aqueous medium and the solution was stirred until the sucrose was completely dissolved. Subsequently, the solution was dried and the remainder was calcined at 600 °C under Ar atmosphere. The samples produced in this way didn't have a uniform and continuous conductive layer, so this method was not used further.

In mechanical method, active material and carbon black with a weight ratio 5:1 were dry ball-milled for 10 h with 200 rpm. Yttria-stabilized zirconia (YSZ) balls were used to prevent contamination. Ball-milling was found to be succesfull in coating the samples. However, an additional heat treatment was required in order to remove the residual stress created by milling. This stress may cause structural defects in the crystal structure. It was released by keeping the samples at 650 °C for 4 h under Ar-5% H_2 atmosphere.

4.6 Electrode Preparation and Cell Assembly

After the cathode active material was synthesized, it was coated with carbon as described in Section 4.5. The carbon coated material was vacuum dried at 120 °C overnight. Then, the dry sample was directly transferred to the glovebox where the cathode paste mixture was prepared. The active material, carbon black and binder were mixed in 84/10/6 ratio, respectively. Polyvinylidene difluoride (PVDF) binder

was used as dissolved in N-methyl pyrrolidinone (NMP). The suspension of all materials was mixed until there is no agglomeration. The positive slurry was then coated on Al foil with 250 μm thickness. Doctor Blade method was used during coating process. After coating the active material, it was dried for 3 h at 120 °C and then further dried under vacuum at 120 °C for 1 day. Then, the positive and negative electrodes were cut into the desired size. Discs having a diameter of 18 mm were cut from the prepared sheet of electrodes. All cathode samples contain 2.6 ± 0.02 mg/cm^2 active material.

After the electrodes and separator are in size, the cells were assembled within a glove box filled with Ar. A glass fiber sheet separator, which has 52 g/m^2 density, and LP-40 electrolyte (Merck) were used to avoid short circuit and provide lithium ion transfer between electrodes. The electrolyte solution was 1M $LiPF_6$ in a mixture of ethylene carbonate (EC) and diethylene carbonate (DEC) in a 1:1 volume ratio. The components were placed in an electrochemical test cell (El-Cell). Besides, sealing of the cell and electrolyte filling is the last steps of assembly.

4.7 Electrochemical Tests

The synthesized cathode active materials were electrochemically characterized after they are assembled in the form of a cell as described in Section 4.6. The cells were charged and discharged with different rates on the Solartron 1480 multi channel battery tester. The charge and discharge rates were 0.05, 0.1 and 0.2 C with different combinations, as tabulated in Table 4.9. Notice that 1 C rate corresponded to 140 mAh/g and 0.05 C rate shows a charge or discharge for 20 h. Because the cells are produced at discharge state, the first step of the galvanostatic test was charging. The cut-off voltage range in galvanostatic charge-discharge tests was 2.0 – 4.8 V vs. Li^+/Li.

4.7.1 Cyclic Voltammetry (CV)

CV is a widely used technique for studying electrode processes. The principle of CV relies on applying continuous cyclic potential to working electrode. While the electrode is subjected to a potential forward and backward between fixed values with a constant sweep rate, the corresponding current is measured. The obtained data is current and plotted as a function of potential, which is called cyclic voltammogram.

Table 4.9. The sequence of charge-discharge regime.

# of Cycles	C rate	
	Charge	Discharge
10	0.05 C	0.05 C
10	0.05 C	0.1 C
10	0.1 C	0.05 C
10	0.1 C	0.1 C
10	0.1 C	0.2 C
10	0.2 C	0.1 C
5	0.05 C	0.05 C
10	0.2 C	0.2 C
10	0.2 C	1 C
10	1 C	0.2 C
10	1 C	1 C
5	0.05 C	0.05 C

The potential is applied to the electrode, starting at a voltage E_1 and sweeping in a linear manner to a value E_2. The potential interval (E_2-E_1) is generally selected so that oxidation and reduction reactions occur in between. E_{pa} and E_{pc} show anodic and cathodic peak potentials. Similarly, i_{pa} and i_{pc} belongs to anodic and cathodic peak currents.

A CV plot gives kinetic and thermodynamic information about the electrode reactions. The information about the reversibility of the anodic and cathodic reactions can be obtained by analyzing the peak voltage and current values in both directions. For a process to be reversible, the following conditions must be satisfied.

I. $\Delta E_p = 0.059/n$

II. $i_{pa}/i_{pc} = 1$

III. i_{pa} and/or i_{pc} is linearly proportional to $\nu^{1/2}$

,where n is number of electrons involved in the redox reaction

ΔE_p is the potential interval (E_2-E_1) in V

i_{pa} and i_{pc} are anodic and cathodic peak currents in mA, respectively

v is the voltage sweep rate or scan rate in V/s

The first and second conditions are easily estimated by a CV graph. The third one is related to the ratio of peak current to sweep rate. The relation between peak current and scan rate is defined with the Randles-Sevcik equation:

$$i_p = 2.69 \times 10^5 \times n^{3/2} \times A \times D^{1/2} \times C \times \nu^{1/2} \quad (4.1)$$

,where A is electrode area in cm^2

D is the diffusion coefficient of electro active species in cm^2/s

C is the bulk concentration of electro active species in $moles/cm^3$

In Li-ion batteries, the basic reaction is based on the motion of Li^+ ions between anode and cathode. Thereby, the diffusion rate of the Li^+ ions within the cathode material directly affects the performance of the battery. In this study, CV was used to investigate the diffusion coefficients of Li^+ ions and the polarization behavior of the active materials. The samples doped with different elements were tested and the obtained data was substituted in the Randles-Sevcik equation.

CVs of the doped samples were recorded using Solartron 1480 multichannel potantiostat. During measurements, different scan rates, 1, 0.1 and 0.05 mV/sec, were used. At first, the cells were scanned in the anodic direction until 4.8 V (E_2) and then the potential was linearly decreased to 2.8 V (E_1) in cathodic direction. The samples are subjected to this cycle twice.

(a)

(b)

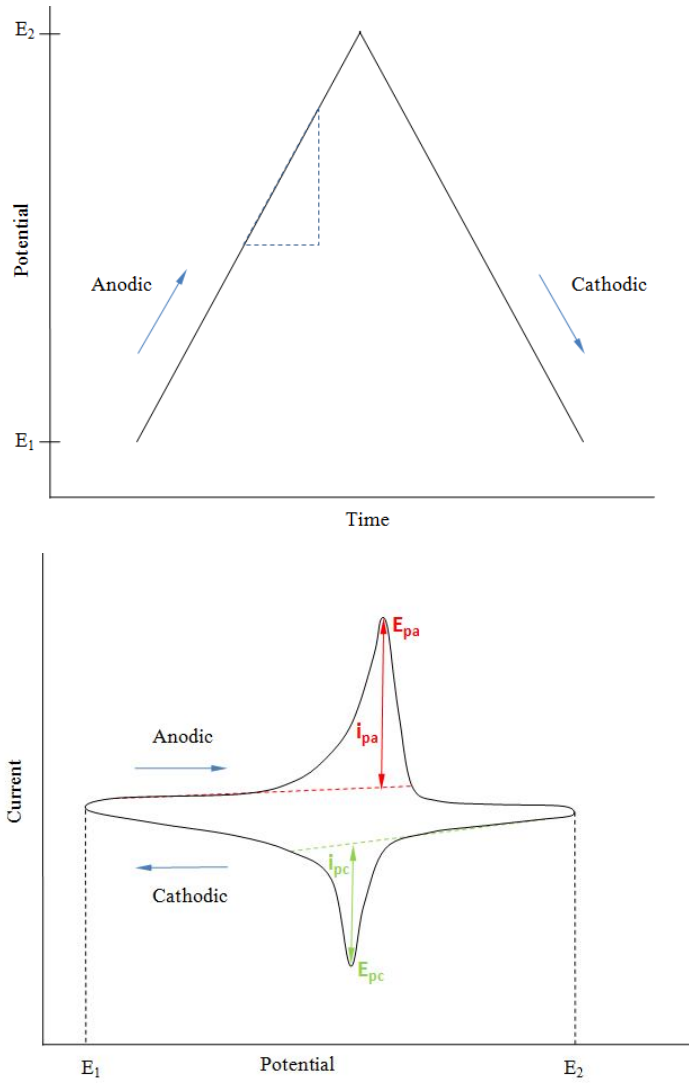

Figure 4.1. (a) Potential wave change and (b) a typical voltammogram representing the important points.

4.7.2 Electrochemical Impedance Spectroscopy (EIS)

EIS method is frequently used to analyze the performance of the batteries in terms of resistance. It also enables analysis and sorting of different types of resistances within a battery. For this purpose, the obtained data are adapted to an equivalent circuit, where the circuit elements express the electrochemical cell.

The model of surface film is the mostly used one for Li-ion batteries, as shown in Figure 4.2. R_{el}, R_{sf} and R_{ct} represent electrolyte resistance, passive surface film resistance and charge transfer resistance, respectively. The circuit elements indicated with Φ shows the capacitive elements; whereas, the term W is related to Li^+ ion motion. Among these elements, resistance elements are the most important ones. R_{el} is directly related to the motion of active ions in the electrolyte solution such as Li^+ ion in Li-ion batteries. R_{sf} stands for the polarization of the passive surface film formed on the electrode surface. R_{ct} is the kinetic resistance of charge transfer in the redox reactions, which makes the battery a power source. Because each cell has the same electrolyte, R_{el} will not change for different experiments. However, R_{sf} and R_{ct} values will give information about the characteristics of the battery.

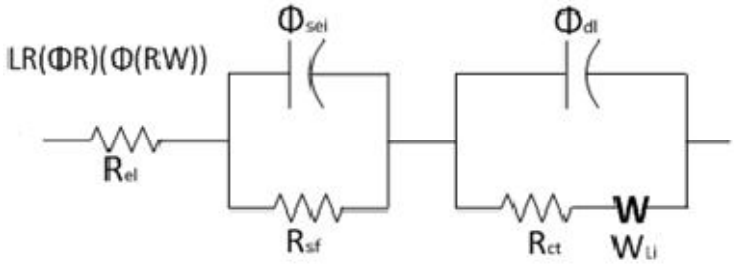

Figure 4.2. The model of surface film.

EIS was performed by applying an AC signal within the frequency range of 300 kHz and 100 mHz. At the open circuit potentials (OCV) of the cells, the AC amplitude of

the potential was ±10 mV. The cells were tested at practical state of charge (SOC) 0 and 100.

CHAPTER 5

RESULTS AND DISCUSSION

5.1 Structural and Morphological Characterization

5.1.1 The Effect of Concentration and Molar Ratio

Generally, the concentration of the starting solution plays a critical role in determining the chemical reaction rate by means of nucleation. In this set of experiments, starting compounds with different molarity; but, the same molar ratio $Li/Mn/PO_4$= 3/1/1 were used. It was expected to have particles with different particle size distributions due to concentration effect. However, as shown in Figure 5.1, there is no sharp difference between samples. As a result of this set, the solution with 0.45 M LiH, 0.15 M MnAT and 0.15 M AmPh or PhAc was determined as the precursor of hydrothermal synthesis.

Following determination of concentration, the molar ratios of the starting solutions need to be optimized. There are many studies showing that a basic medium is desired for the formation of olivine type phosphates [25]. In order to create the required ambient, one idea is to add excess amount of lithium hydroxide and the other is to place a basic non-reactive agent into the reaction medium.

Li, Mn and PO_4 source solutions with molar ratios of 3/1/1, 3/2/1 and 1.2/1/1 were prepared and hydrothermally reacted. After the obtained powders were analyzed, it is observed that some undesired phases formed with LMnP. First, the starting solutions having highly excess amount of LiH resulted in the formation of Li_3PO_4. The quantitative results of the samples are given in Table 5.1. Secondly, the samples produced with excess MnAT contain different types of manganese compounds such as Mn_2PO_5, $Mn_3P_2O_8$ and $LiMn_2O_4$. The diffraction data of these samples were so complex; therefore, accurate quantitative analysis could not be done. Thirdly, the phase analysis of 1.2/1/1 sample produced with PhAc shows that it contains 5.8% $Mn_5(PO_3OH)_2(PO_4)_2{\cdot}4H_2O$ (MPH) and 94.2% LMnP by weight; whereas, the one produced with AmPh consist of 100% LMnP by weight.

There are two distinct results of this experiment set. The first one is that excess Li^+ and Mn^{3+} ions in the reaction medium interact with PO_4^{3-} and form stable phosphate compounds. Therefore, it is noted that highly excess precursors should not be used. The other one is the formation of MPH. It is a mineral known as Hureaulite and formed in hydrothermal medium. This compound was thought to be an intermediate product of the LMnP formation sequence. Because this phase formed in the experiment where PhAc was used, it may be a phase that is stable at low pH. The XRD diffraction patterns of LMnP with Li_3PO_4 and MPH are shown in Figure 5.2 (a) and (b), respectively.

Table 5.1. Quantitative phase analysis of molar ratio samples

Sample Name	LMnP (% by weight)	Undesired phase (% by weight)
3/1/1 with AmPh	71.9	Li_3PO_4, 28.1
3/1/1 with PhAc	73.32	Li_3PO_4, 26.28
1.2/1/1 with AmPh	100	-
1.2/1/1 with PhAc	94.2	MPH, 5.8

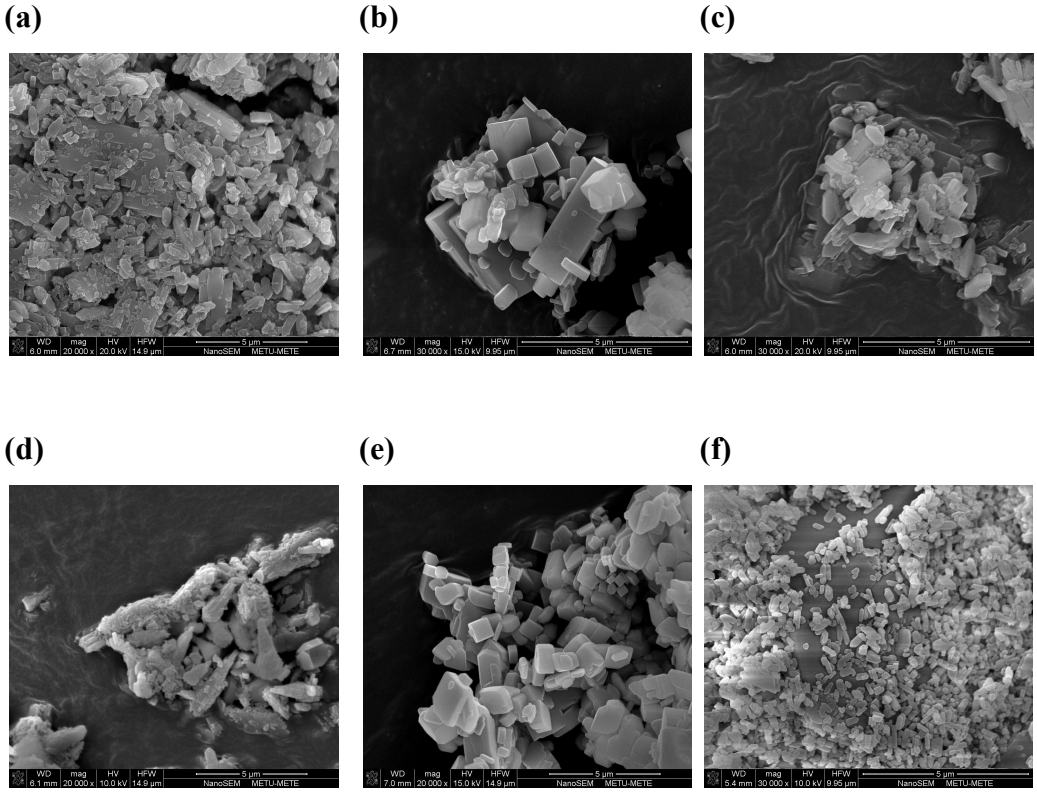

Figure 5.1. SEM images of samples synthesized with different precursor concentrations of (a) 0.15 M with AmPh, (b) 0.15 M with PhAc, (c) 0.3 M with AmPh (d) 0.3 M with PhAc, (e) 0.45 M with AmPh, (f) 0.45 M with PhAc.

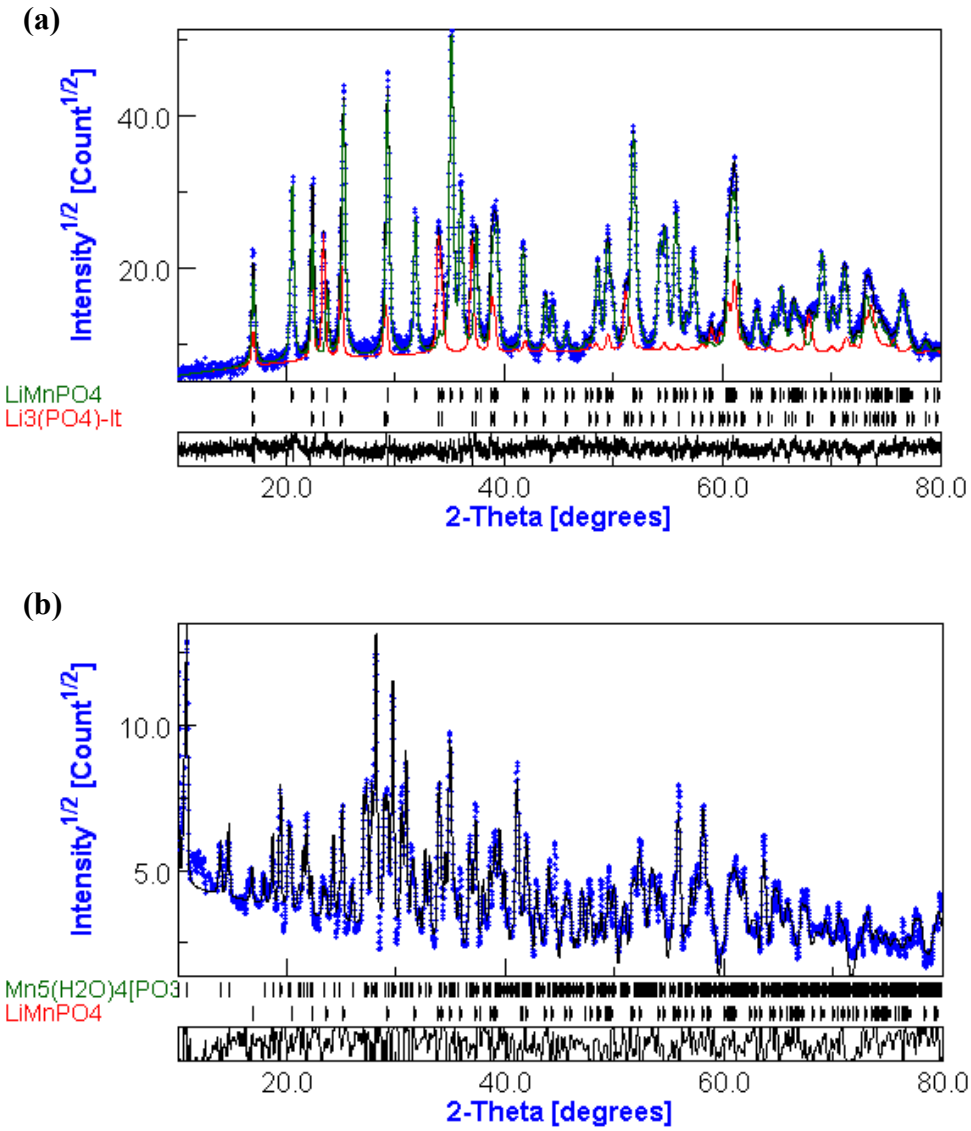

Figure 5.2. XRD patterns of LMnP with (a) Li_3PO_4 and (b) MPH.

5.1.2 The Effect of pH

In literature, excess amount of LH is used to create a basic medium. However, in the concentration experiment set, it is understood that excess amount of Li^+ reacts with PO_4^{3-} forming undesired phases. Consequently, Li ratio was lowered to remove the excess amount. Also, using PhAc as PO_4 source was left because it decreased pH of the medium.

Experiments at different pH values were conducted and the pH of the medium was adjusted by adding 25% ammonia solution. The ammonia solution was added to the precursor before it was placed into the hydrothermal reactor.

The results show that both low and high pH values caused the formation of electrochemically inactive phases. pH lower than 10 caused the formation of MPH while $NH_4MnPO_4 \cdot H_2O$ (NMPH) phase was formed at a high pH. The weight percentages of the existing phases are tabulated in Table 5.2. MPH formation at low pH values was also coherent to the results of molar ratio experiments.

Table 5.2. Phase analysis results of pH experiments.

pH	LMnP (% by weight)	Undesired phase (% by weight)
<10	15.3	84.7
≈ 10	100	-
>10	39.8	60.2

NMPH, named as niahite, is a mineral with orthorhombic system and $Pmn2_1$ space group. In Figure 5.3, it is seen that it has a similar crystal structure to LMnP. NH_4^+ ions replace with Li^+ ions in the LMnP structure. The source of these NH_4^+ ions is the ammonia solution, which was used to increase pH. The diffraction pattern of the sample synthesized with the presence of ammonia solution is given in Figure 5.4 and it shows a characteristic peak of NMPH around 10°. After quantitative analysis of all samples, the optimum thermodynamic condition for the formation of LMnP phase was eventually determined as $pH \approx 10$.

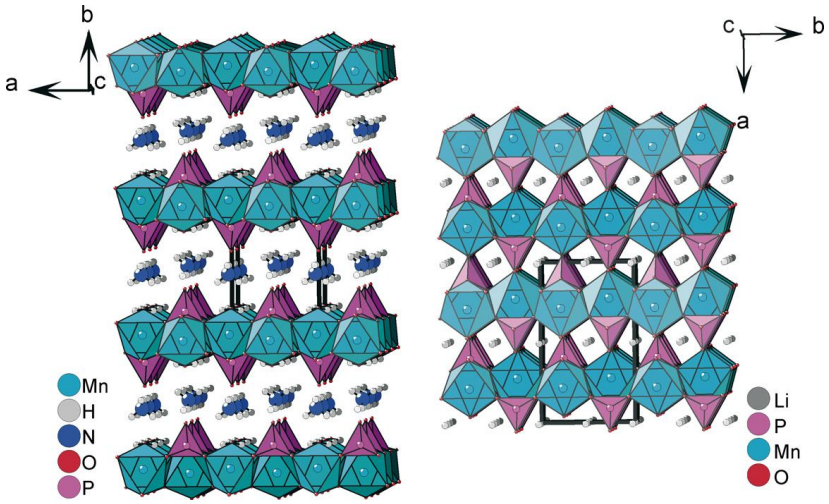

Figure 5.3. The crystal structures of NMHP (left) and LMnP (right) [30].

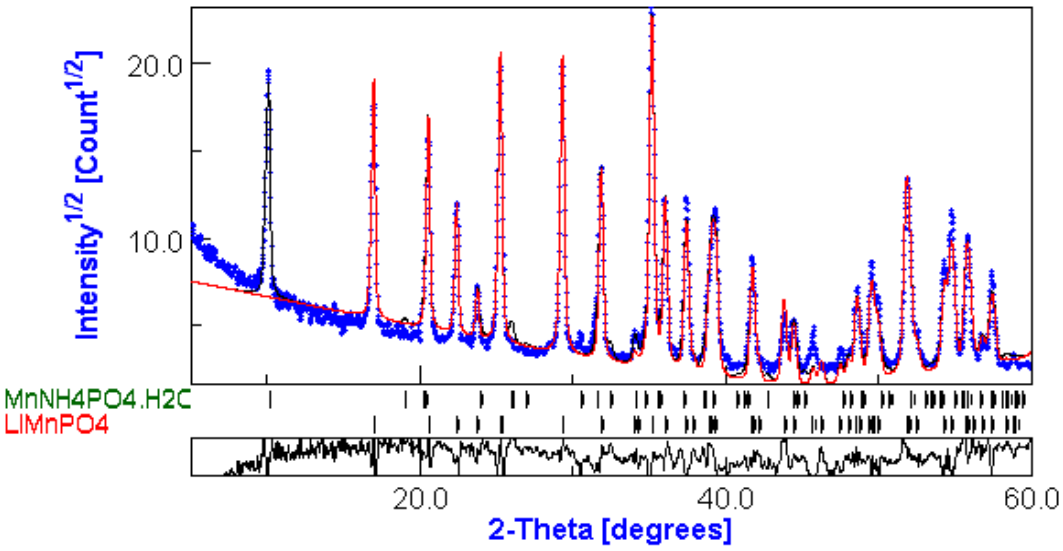

Figure 5.4. XRD pattern of LMnP with NMPH.

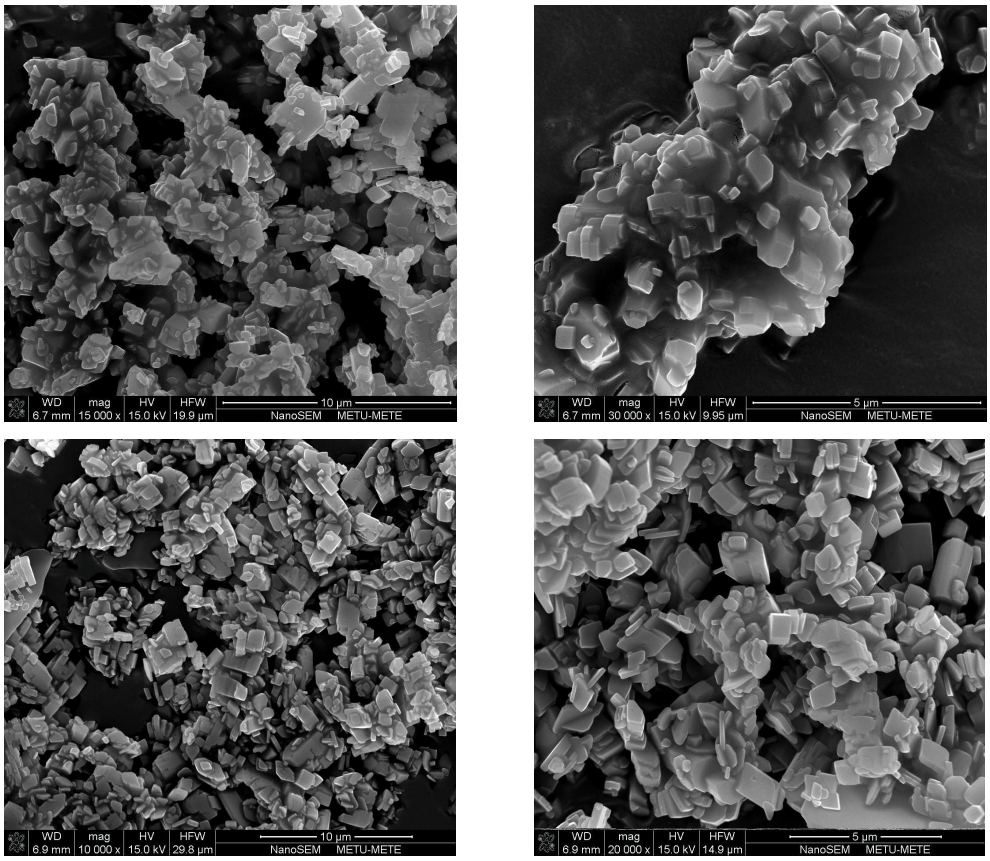

Figure 5.5. SEM images of synthesized powders including large amounts of (a) MHP and (b) NMPH phases.

5.1.3 The Effect of Time

The reaction time is vital for phase formation and particle size distribution. There is a time limit where the formation reaction of LMnP is completed and the particles keep growing if continued. Moreover, as time passes, some compounds may decompose and cause to form other undesired phases according to the reaction sequence and phase stability intervals. In order to find that critical point for pure LMnP, different durations of reaction were studied. The precursor mixtures under the same conditions were reacted at 200 °C for 240, 480 and 600 min.

Quantitative phase analysis show that each sample contain 100% LMnP with no foreign phase. However, the particle size distributions vary because of the noticeable difference in the reaction times. As seen in Figure 5.6, the longer the particles were kept at high temperature, the bigger the particles get. Moreover, SEM images of samples prove that increasing reaction time results in bigger and smoother particles, Figure 5.7. The particles have tendency to cluster and combine from coherent edges or sites, when the required driving force exists.

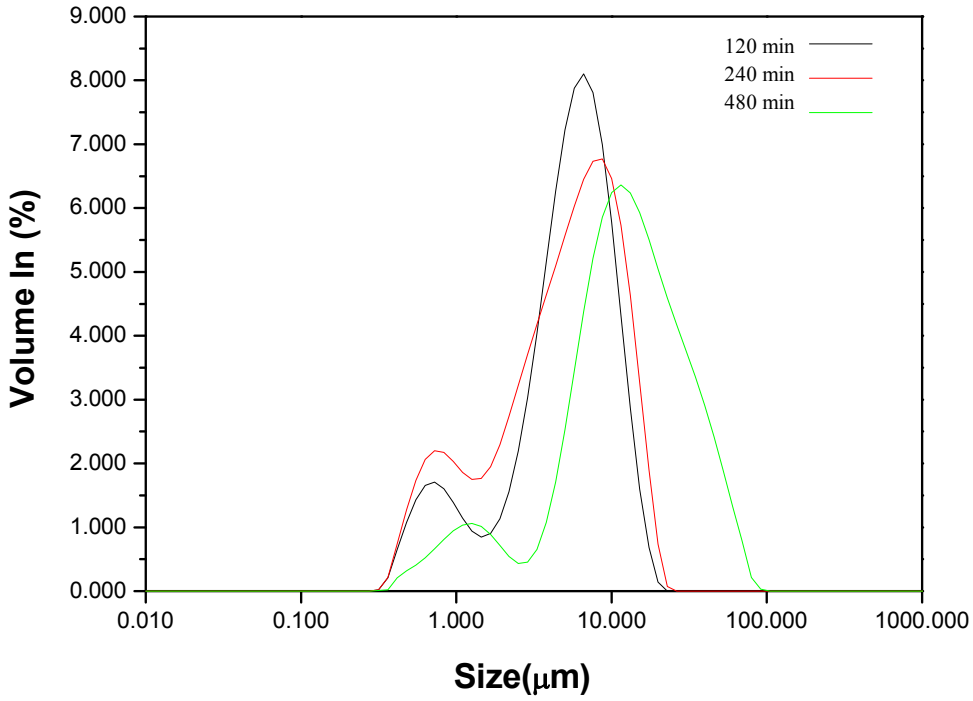

Figure 5.6. Particle size distribution of samples reacted for 120, 240 and 480 min.

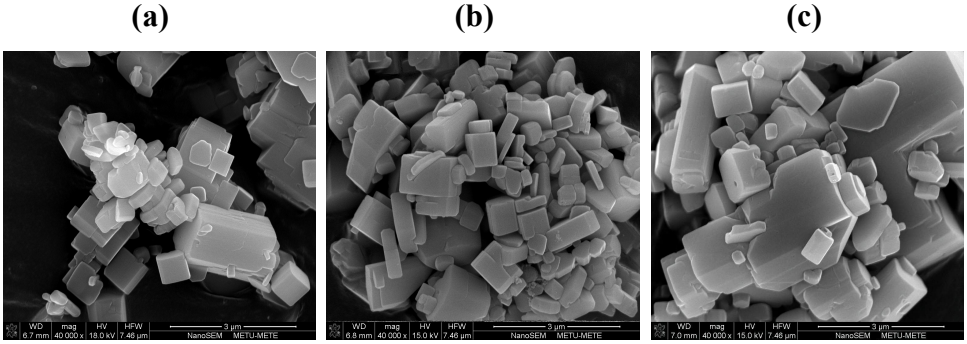

Figure 5.7. SEM images of samples reacted for (a) 240, (b) 480 and (c) 600 min.

5.1.4 The Effect of Temperature

The effect of temperature was investigated with the set of experiments seen in Table 4.6. The samples were synthesized at 120, 150 and 200 °C. XRD analysis of both 120 °C and 150 °C samples gave complex patterns, which did not allow quantitative phase analysis. However, as the patterns were searched-matched, a list of possible phases were determined that are Mn_2PO_5, $Mn_3P_2O_8$, $LiMn_2O_4$ and $Li_8Mn_{17}O_{32}$.

As shown in Table 5.3, the samples synthesized at 120 and 150 °C have 87.3 % and 18.75% MPH by weight, respectively. On the other hand, the powder synthesized at 200 °C only consists of LMnP phase. As a results, it is seen that increasing reaction temperature increases LMnP amount and prevents the formation of MPH.

Table 5.3. The phase analysis of temperature set.

Temperature °C	LMnP (% by weight)	MPH (% by weight)
120	12.7	87.3
150	80.25	18.75
200	100	-

5.1.5 The Effect of Additives

In this study, different additives were used to understand their effect on the synthesis of LMnP particles. At first, GLU and LA, which act as carbon source and reducing agent, respectively, were used. They increase the carbon amount in the medium and prevent the oxidation of Mn^{2+} ions. Afterwards, the effect of CA was investigated. CA is a chelating agent increasing the stability of metal ions and thus inhibits the formation of undesired compounds. Furthermore, anionic and cationic surfactants were used. They were CTAB, a well-known cationic surfactant, and SDS, an anionic surfactant. In the following studies, some commercial surfactants and thickening agents such as PEG, PVA and GEL were used.

Phase analysis results of the samples synthesized with the presence of additives are tabulated in Table 5.4. XRD patterns are shown in Figure 7.1 in Appendix and the analyses of the samples revealed that nearly all patterns, except CA, PVA and LA, have a clear peak around 10° which is a characteristic peak of NMPH. The reason of the formation of this phase is the excess ammonia solution that was added to adjust the pH.

Table 5.4. Phase analysis of the samples synthesized with additives.

	LMnP (% by weight)	NMPH (% by weight)
GLU	76.15	23.85
CA	100	-
EG	88.22	11.78
CTAB	92.46	7.54
SDS	66.34	33.66
PEG	94.34	5.66
PVA	100	-
IGE	75.11	24.89
GEL	91.47	8.53
LA	100	-

SEM images of the samples in Figure 5.8 prove that different additives result in diverse powder topographies with preferred orientations. However, the aim was to decrease the particle size and it couldn't be achieved.

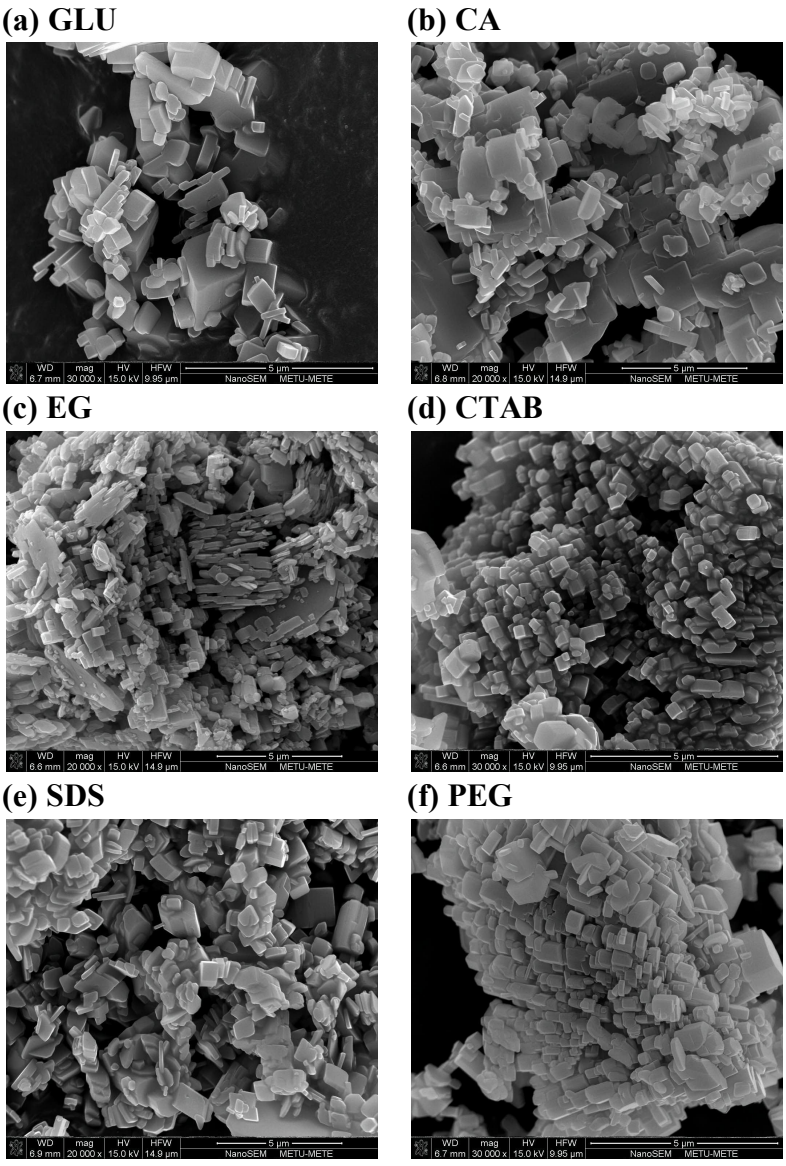

Figure 5.8. SEM images of the samples synthesized with additives.

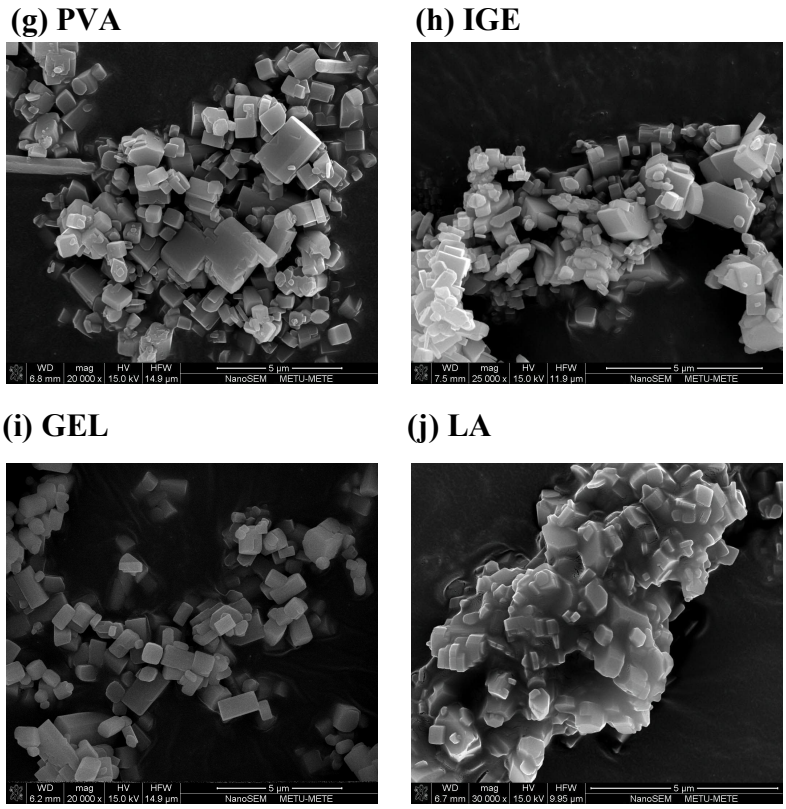

Figure 5.8. (Continued)

As a result, the optimum reaction parameters of pure LMnP were fixed as shown in Table 5.5. The doping experiments were conducted according to these values. Plus, the XRD pattern of olivine type LMnP powder synthesized with these conditions is provided in Figure 5.9.

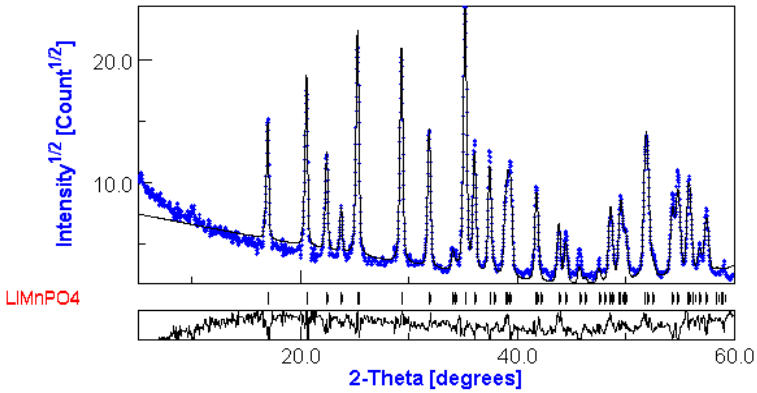

Figure 5.9. The XRD pattern of pure LMnP.

Table 5.5. The optimum reaction parameters of LMnP.

Li source	LiH
Mn source	MnAT
PO_4 source	AmPh
Mn concentration	0.15 M
pH	≈10
Molar Ratio	Li/Mn/PO_4=1.2/1/1
Temperature	200 °C
Time	240 min
Additive	None

5.2 Doping LMnP Structure with Doping Elements

The synthesized powders were first analyzed by XRD and the patterns are provided in Figure 7.2 in Appendix. The samples showed no peak of undesired phases rather than LMnP. Because the doped compounds have olivine structure, it is expected to have the same patterns with slight shifts in the peak positions. It is because, the replacement of an atom with another one having different atomic radius changes the lattice parameters. The lattice parameters were calculated by the Rietveld Method and provided in Table 5.6.

Table 5.6. Lattice parameters of doped samples.

Alloying Element	**R_w**	**a (Å)**	**b (Å)**	**c (Å)**
Pure	19.80	10.453	6.099	4.751
Co	17.00	10.443	6.088	4.747
Cr	19.35	10.454	6.098	4.752
Mo	21.81	10.448	6.095	4.748
V	18.85	10.54	6.097	4.752
W	20.19	10.451	6.095	4.749

In order to understand whether the dopants substitute the lattice atoms, elemental analyses were conducted. The elemental analysis results in molar percentage are given in Table 5.7. When the elemental molar ratios are investigated, it is observed that dopants substitute the lattice atoms in the structure.

Table 5.7. EDX analysis of the doped samples.

Elements	HT- W5	HT- V5	HT- Co5	HT- Cr5	HT- Mo5
Mn	48.65	52.85	48.43	47.85	44.15
P	29.61	26.73	30.03	30.06	30.97
O	20.35	19.61	18.99	21.41	24.57
Dopants	1.41	0.8	2.55	0.67	0.31

5.3 Electrical Test Results

The electrical conductivity of the samples was measured and the values were calculated from the slope of the related I-V graphs. For instance, the I-V graph of pure LMnP is given in Figure 5.10. The conductivity of undoped LMnP was found as 3.36×10^{-11} S/cm at room temperature. This value is quite lower than 2.7×10^{-9} S/cm, which was measured at 300 °C [17]. If the difference in the measurement temperature is considered, the obtained conductivity value of the sample becomes more reasonable.

The electrical conductivity results of doped samples are tabulated Table 5.8. It is clearly seen that doping with alloying elements has an improving effect on the electrical conductivity. Especially, the samples doped with Co and V have nearly one order of magnitude higher electrical conductivity values than just plain LMnP.

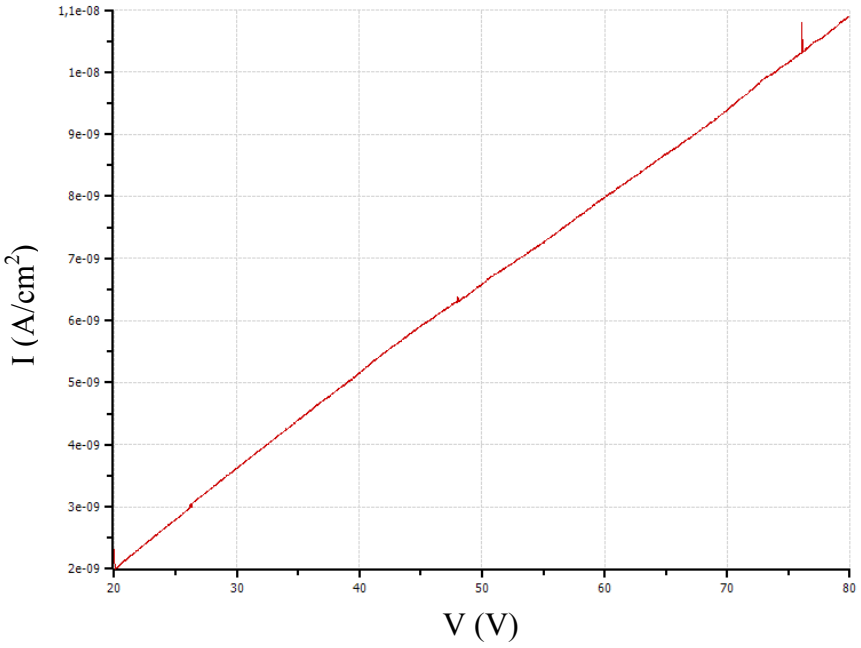

Figure 5.10. The I-V graph of the undoped sample.

Table 5.8. Electrical conductivity values of undoped and doped samples.

Sample Name	**Electrical Conductivity (S/cm)**
Undoped	3.36×10^{-11}
HT-Co-5	1.01×10^{-10}
HT-Cr-5	5.92×10^{-11}
HT-Mo-5	3.29×10^{-11}
HT-V-5	6.68×10^{-10}
HT-W-5	4.32×10^{-11}

5.4 Carbon Coating

Ball-milling method was used to uniformly coat the particles with carbon and also to decrease the particle size. SEM images of the milled samples are provided in Figure 5.11 (a1)- (f1). It is seen that as-milled particles are smaller in size and the sharp edges of the particles are rounded. Afterwards, in order to remove the residual stress caused by ball milling and crystallize the partially amorphous structure, the samples were heat treated at 650 °C for 4 h under Ar-%5 H_2 atmosphere. If the samples before and after the heat treatment are compared, it is seen that they differ in size and shape. The small particles obtained by ball-milling formed agglomerates with 5-10 μm size after heat treatment, Figure 5.11.

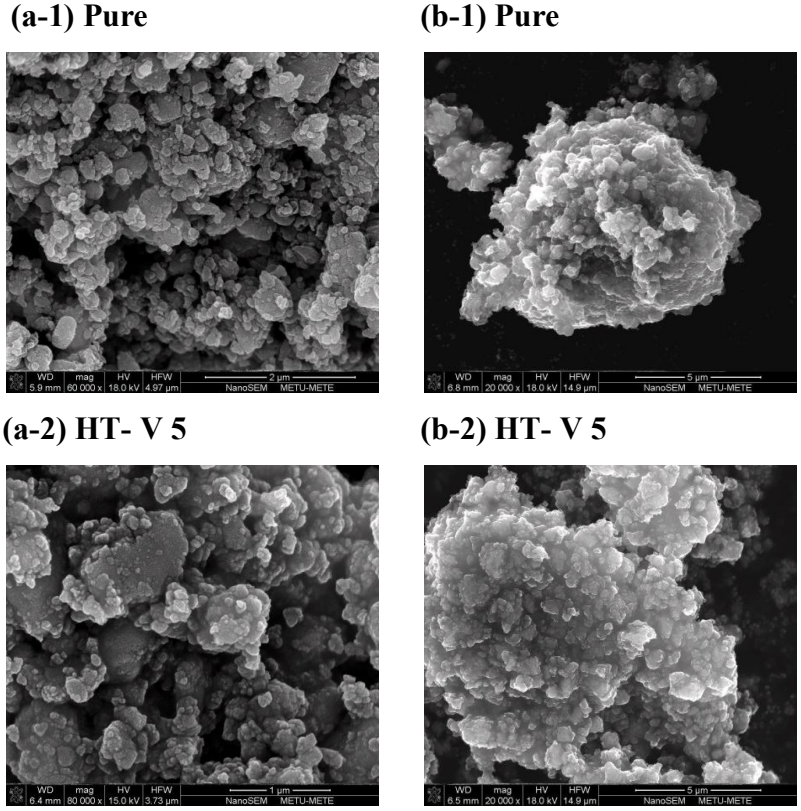

Figure 5.11. SEM images of pure and doped samples after ball milling (a) 1-6 and heat treatment (b) 1-6.

(a-3) HT-Cr 5

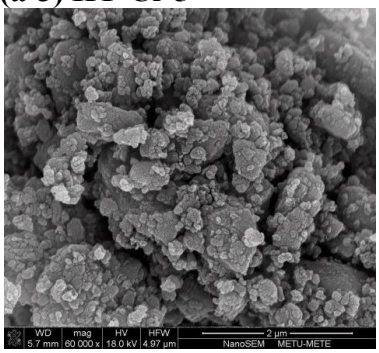

(b-3) HT-Cr 5

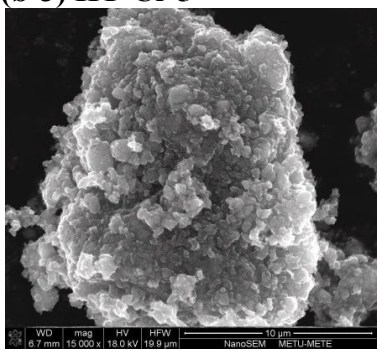

(a-4) HT-Co 5

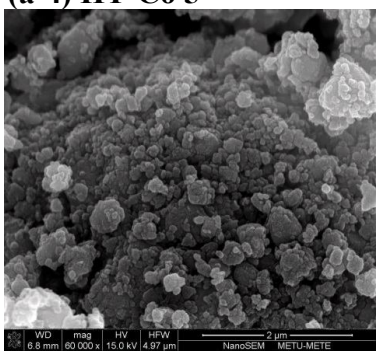

(b-4) HT-Co 5

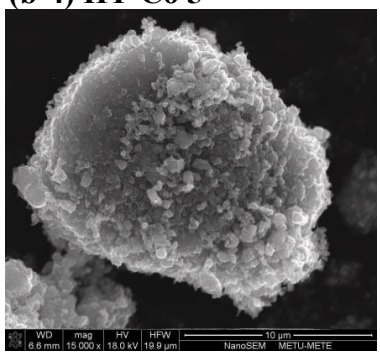

(a-5) HT-Mo 5

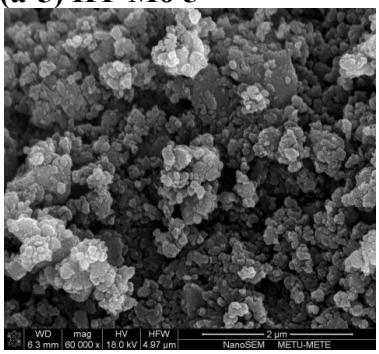

(b-5) HT-Mo 5

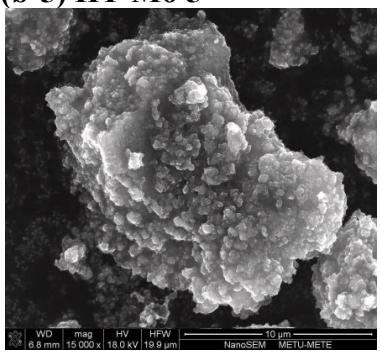

(a-6) HT-W 5

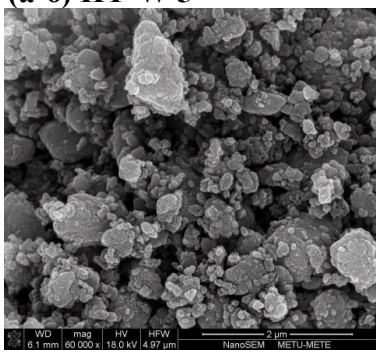

(b-6) HT-W 5

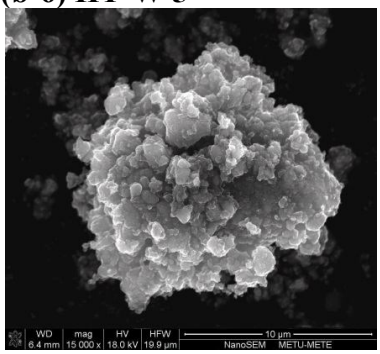

Figure 5.11. (Continued)

5.5 Electrochemical Test Results

The cells with synthesized LMnP cathode were charged and discharged for several times. The discharge capacity vs cycle number plot is seen in Figure 5.12. This plot shows that produced LMnP cathode materials have a capacity around 70 mAh/g which is quite higher than literature values [22]. Moreover, it is seen that there is no obvious decrease in the capacity when the cells are charged fast. If the plot of pure sample (dark blue) is compared with the others, the effect of dopants is understood. As cycle number increases, the capacity fade of the pure sample dramatically increases, especially at high charge-discharge rate. However, the capacity of Co and V doped samples decrease in an acceptable manner as cycle number increases. On the other hand, the cell with Cr doped LMnP gives the best performance in rate capability. Although it has low capacity, it steadily gives its capacity even at high rates.

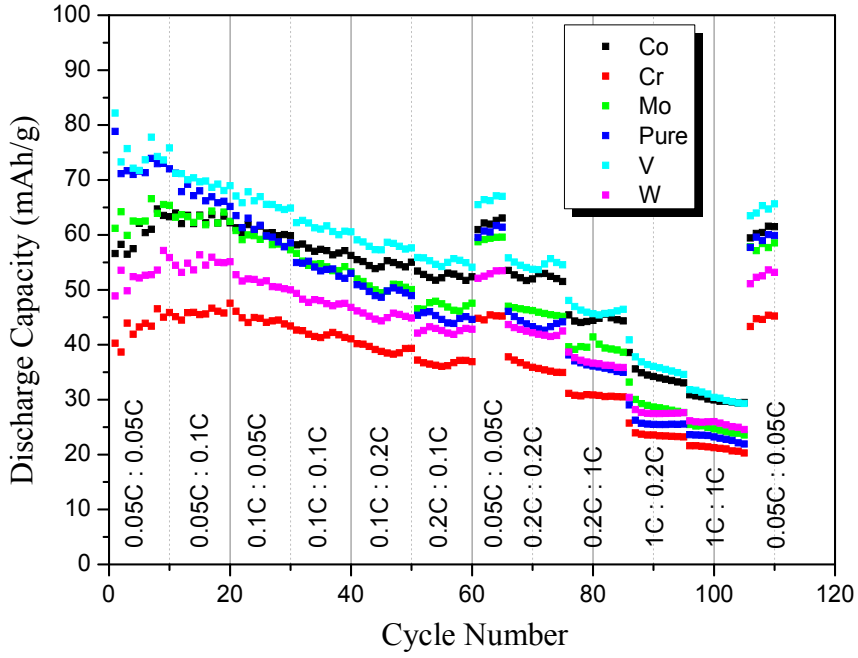

Figure 5.12. The capacity of discharge and rate capability graph.

The voltage profiles of pure and doped samples are given in Figure 5.13 (a)-(f). As seen in the profiles, the samples show a plateau around 4.1 V. Nevertheless, the cells with Co and V doped LMnP keep their capacity and voltage profile almost unchanged at moderately high rates.

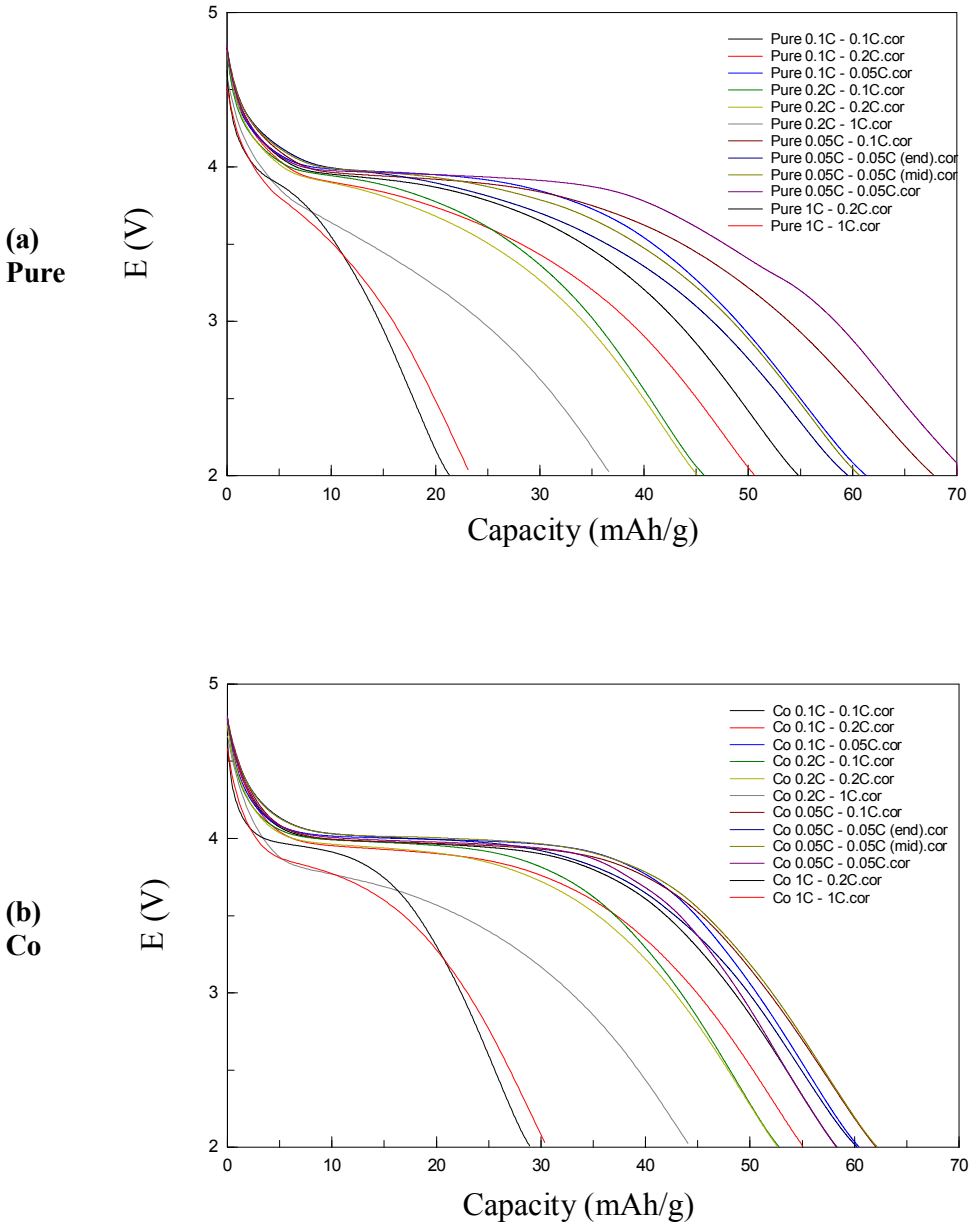

Figure 5.13. The voltage profiles of the samples.

(c)
Cr

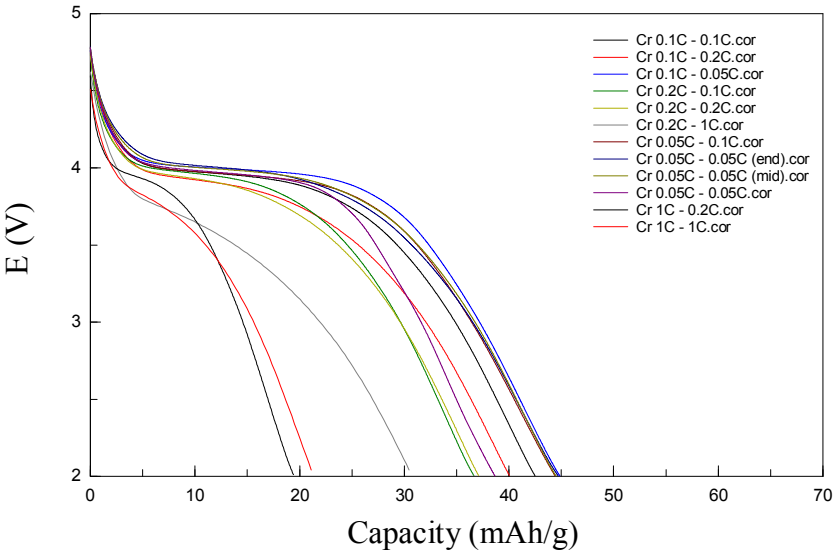

(d)
Mo

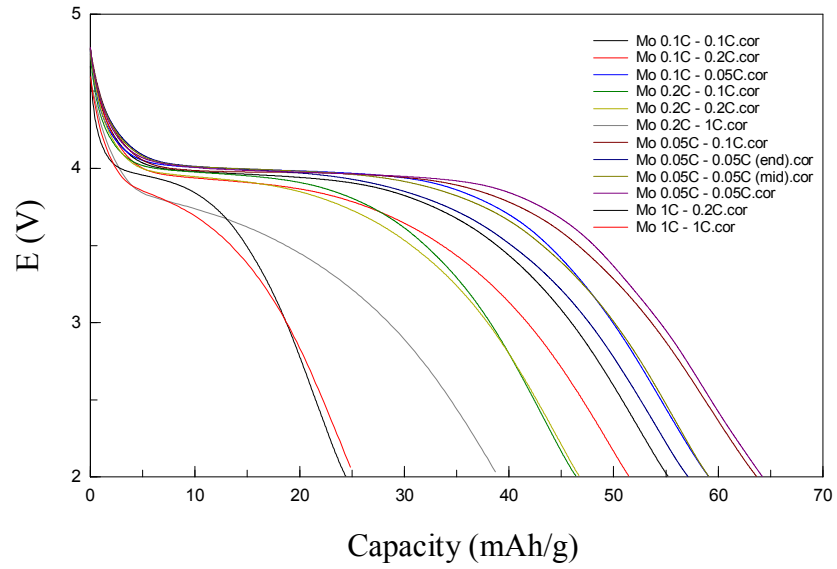

Figure 5.13. (Continued)

(e)
V

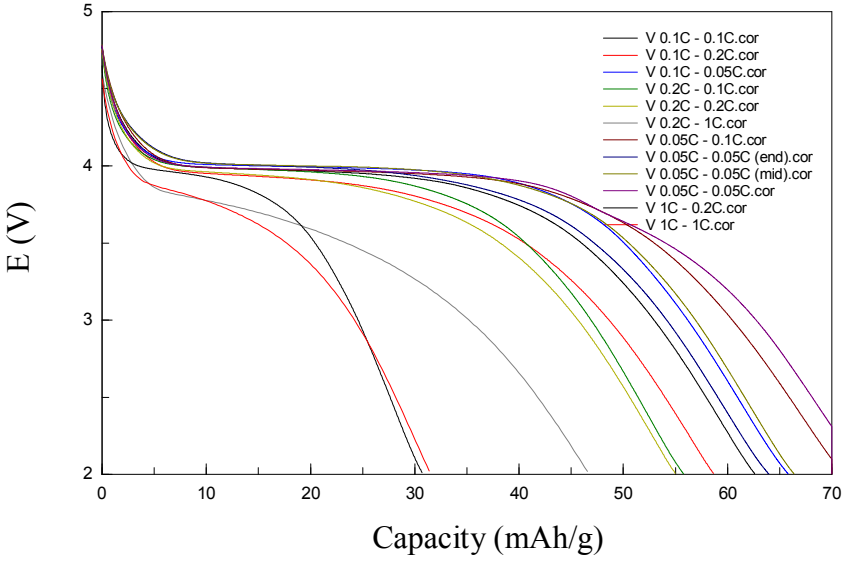

(f)
W

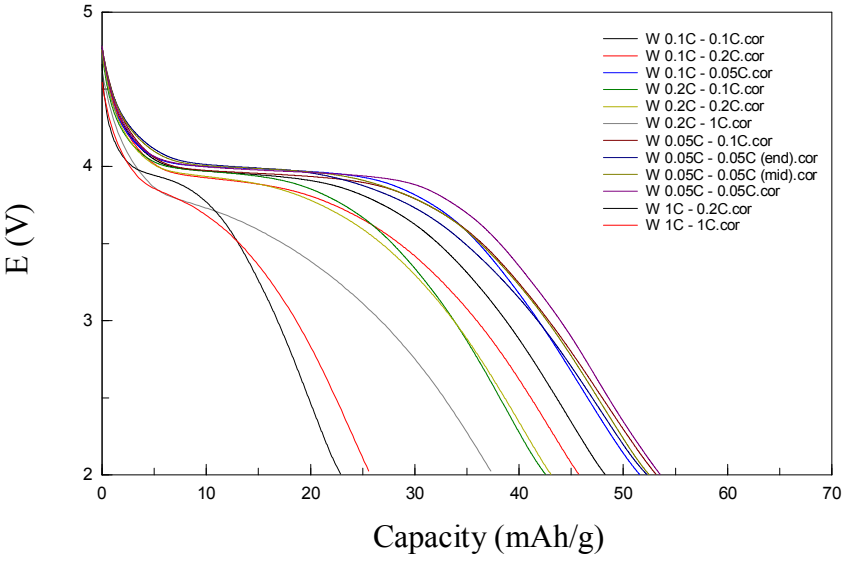

Figure 5.13. (Continued)

5.5.1 CV Measurements

The reversibility of the reactions and the kinetics of Li^+ ion motion within cathode active materials were analyzed by measuring peak points on CV graph. The plots of the cells having undoped and doped LMnP are given in Figure 5.14 (a)-(f).

(a) Pure

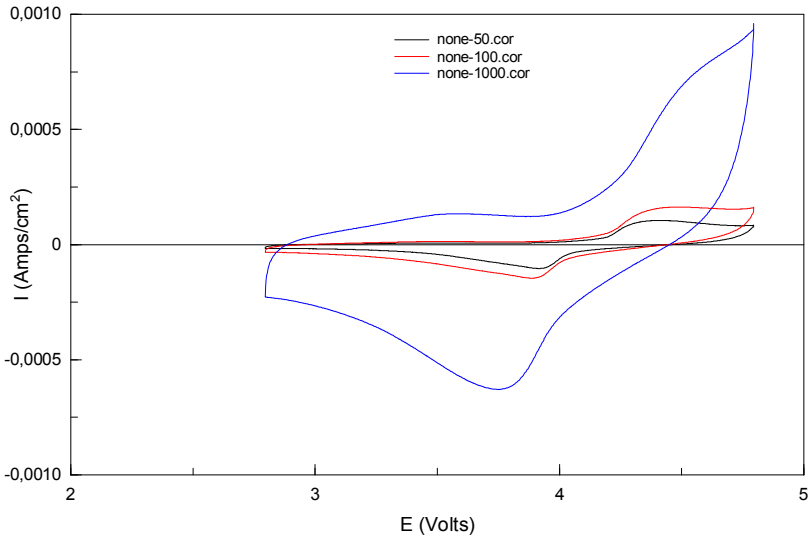

(b) Co

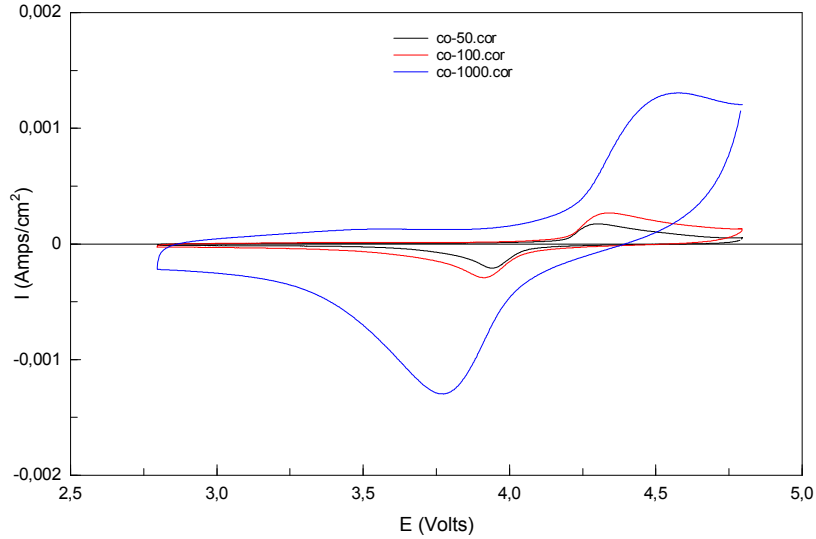

Figure 5.14. CV plots of cells with pure and doped LMnP.

(c) Cr

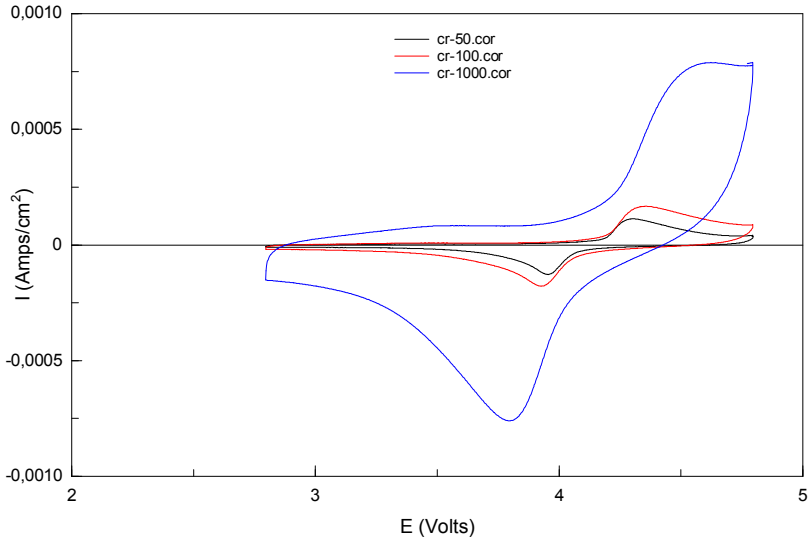

(d) Mo

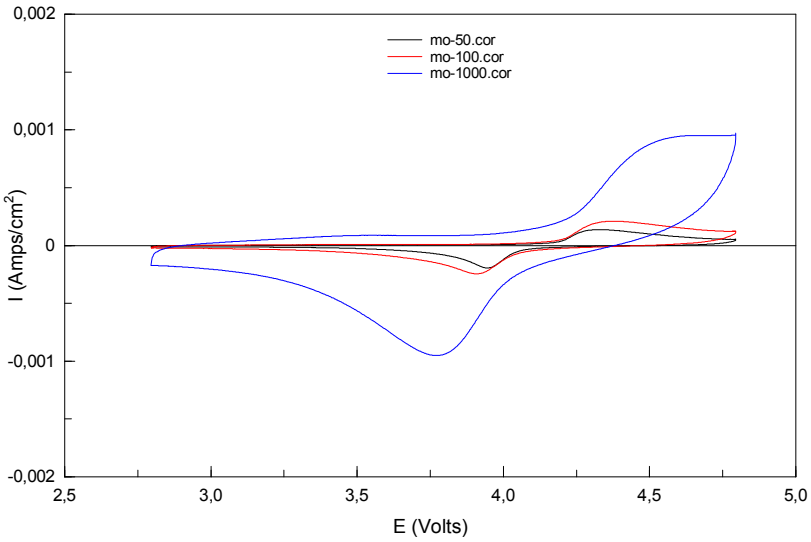

Figure 5.14. (Continued)

(e)
V

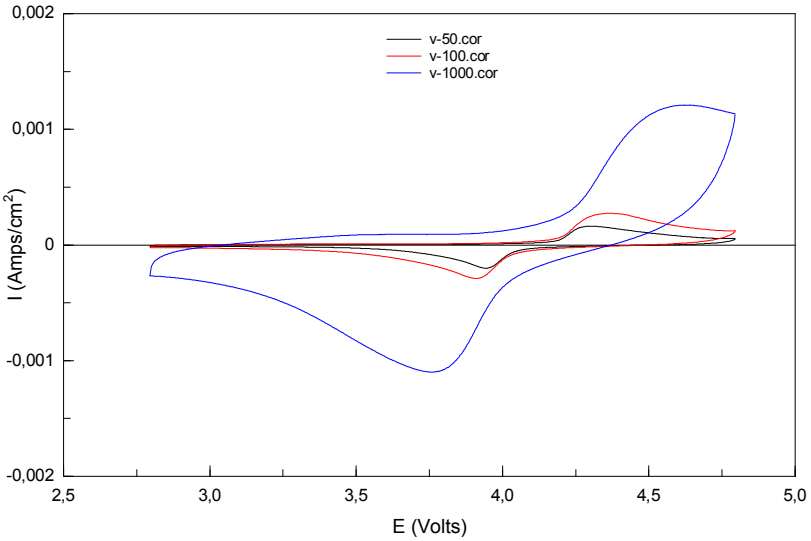

(f)
W

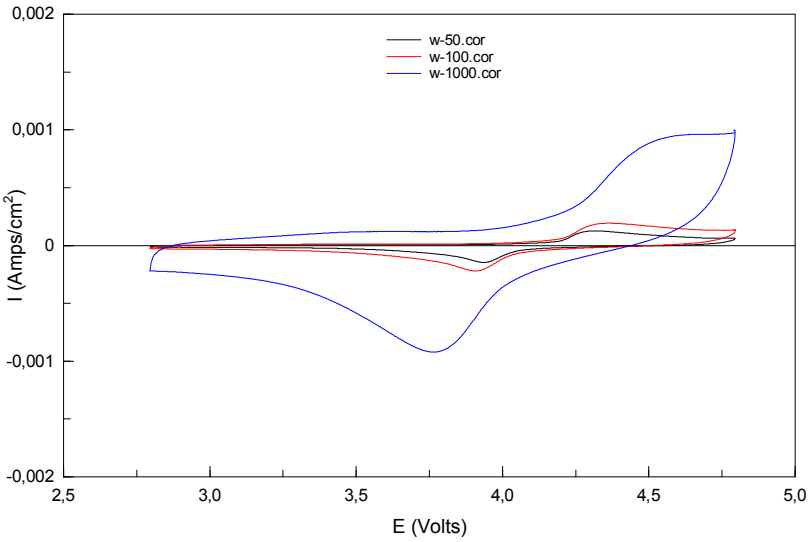

Figure 5.14. (Continued)

The samples are scanned with different scan rates and the the anodic and cathodic peak values of current and voltage are measured. At first, the reversibility is studied by using the potential interval (ΔE_p) data. As described in Section 4.7.1, when the number of electrons involved in the reaction is 1, ΔE_p should be equal to 0.059 V. In thermodynamic point of view, the slowest rate gives the most accurate ΔE_p; therefore, the values at 50 μV/s were compared, Table 5.9. The reversibility of reactions in the cells having doped LMnP is not satisfactory. However, when the undoped and doped samples are compared, the positive effect of doping on the reversibility is seen, especially for Co, Cr and V. Secondly, the diffusion coefficients of Li^+ ion in different cathode active materials were calculated using Randles-Sevick equation because diffusivity plays a critical role in quick charging and efficiency. The calculated values are given in Table 5.10. Doping LMnP with Co and V considerably increases the diffusion coefficient of Li^+ ion, which is desired for a better battery performance.

Table 5.9. ΔEp values of doped samples at different scan rates.

Scan rate (μV/s)	Undoped	Co	Cr	Mo	V	W
1000	0.7882	0.8075	0.8244	0.8898	0.876	0.9205
100	0.6063	0.4269	0.4297	0.4665	0.4521	0.4583
50	0.4957	0.3552	0.3509	0.3803	0.358	0.3776

5.5.2 EIS Measurements

The results of EIS are given in Figure 5.15. The measured impedance is mathematically fitted to surface film model and the values of the resistance elements are calculated and provided in Table 5.11. As anticipated in Section 4.7.2, R_{el} values are similar for all of the samples because the same electrolyte solution is used. Also, the samples show similar surface film characteristics. This result corresponds to the

polarization behavior obtained by CV. On the other hand, R_{ct} values vary between samples. It is seen that the alloying elements decrease the resistance of charge transfer which is quite high for pure undoped LMnP. Especially Co doped cathode performs best among the other alloying elements.

Table 5.10. The diffusion coefficients of doped samples in anodic (Li deintercalation) and cathodic (Li intercalation) directions.

	Diffusion Coefficients (cm^2/sec)	
	Anodic	**Cathodic**
Undoped	3.887×10^{-11}	2.789×10^{-11}
Co	1.296×10^{-10}	1.203×10^{-10}
Cr	4.619×10^{-11}	4.054×10^{-11}
Mo	6.662×10^{-11}	5.854×10^{-11}
V	1.078×10^{-10}	8.026×10^{-11}
W	7.064×10^{-11}	6.003×10^{-11}

Table 5.11. The values of R_{el}, R_{sf} and R_{ct} calculated by the surface film model, SOC=0.

	R_{el} (ohm)	**R_{sf} (ohm)**	**R_{ct} (ohm)**
Undoped	14.98	24.21	2.598×10^{14}
Co	15.43	22.07	8.694×10^{4}
Cr	19.53	23.46	1.383×10^{10}
Mo	16.50	19.27	1.331×10^{11}
V	15.47	22.43	6.883×10^{9}
W	15.93	22.35	1.672×10^{9}

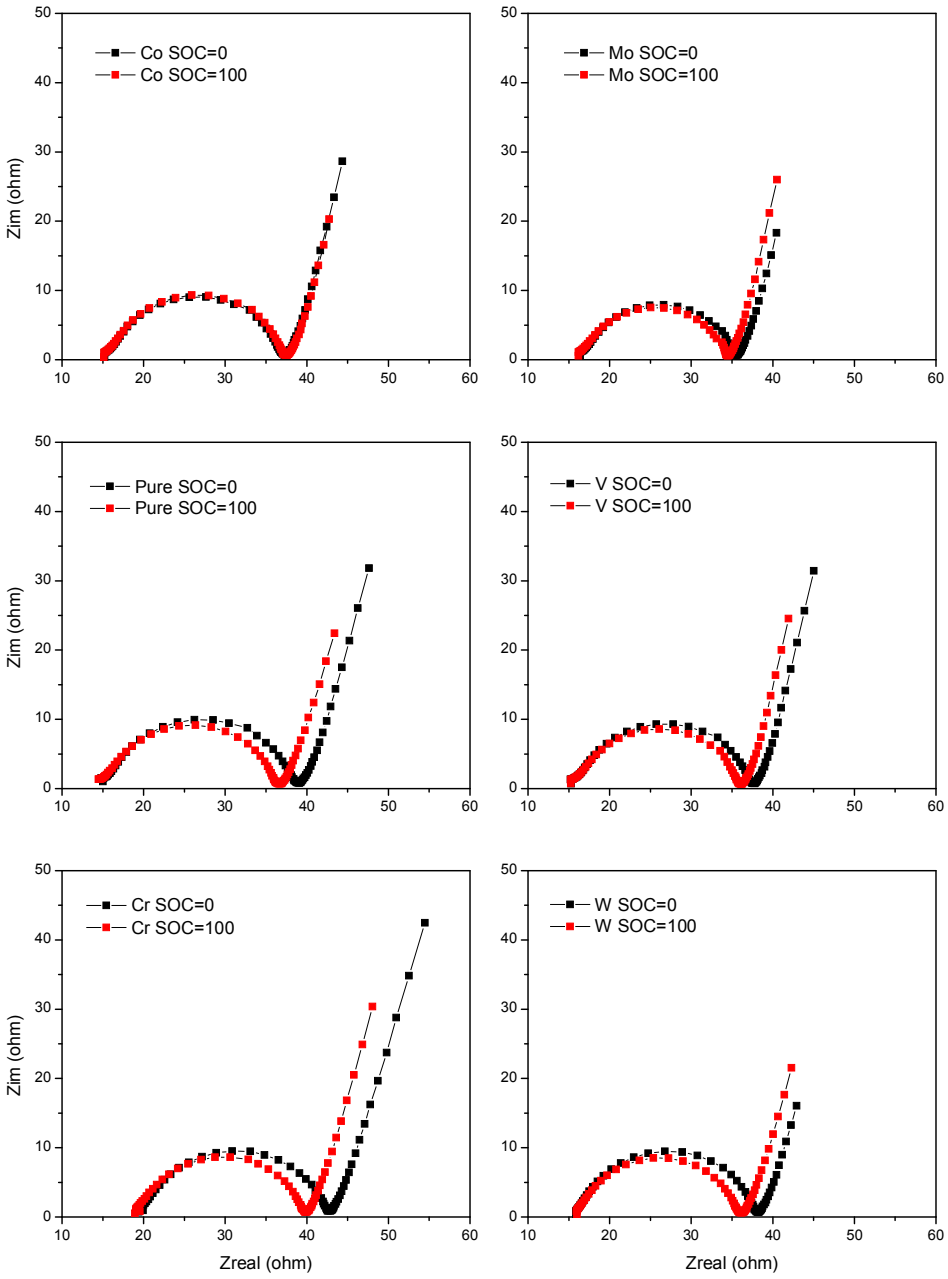

Figure 5.15. Nyquist impedance plots of LMnP.

CHAPTER 6

CONCLUSIONS

The purpose of this study was to synthesize a specific cathode active material, LMnP, and its doped versions by hydrothermal method and characterize them in terms of structure and electrochemical performance. Also, different approaches such as decreasing particle size, coating the particles with a conductive carbon layer and doping were investigated in order to eliminate the poor conductivity features of LMnP.

Firstly, in order to find the optimum synthesis parameters for pure LMnP, many experiment sets were designed. Each variable was investigated within an experiment set by keeping other parameters constant. The parameters were grouped and investigated in the order of increasing effect to the reaction kinetics. The first parameters to study were concentration and molar ratio. It is seen that excess amounts of precursor chemicals affect the medium and enable the formation of impurity phases. Then, the optimum molar ratio was found as $Li/Mn/PO_4$= 1.2/1/1 with 0.15M Mn concentration. Afterwards, the reaction time and temperature were studied. They both excessively affect the particle size of the synthesized powders. After structure and morphology of the samples were analyzed, LMnP synthesized at 200°C for 2h gave the best results of particle size distribution. Also, during powder preparation, it was understood that the control of the pH plays a critical role in the

formation of final product. pH values less than 10 caused the formation of MHP phase; whereas, NMPH phase is formed at a pH value higher than 10. It is understood that the reason why NMPH phase formed is the ammonia solution used to increase the pH of the reaction medium. Then, the optimum pH was fixed to 10.

After the boundary conditions of LMnP synthesis were determined, doped samples with the formula $LiMn_{0.95}M_{0.05}PO_4$ were synthesized. For doping, Co, Cr, Mo, V and W were used. In order to be sure that the Mn-site in the structure is doped with the given elements, the samples were analyzed with XRD (Rietveld Refinement) and EDX.

The synthesized powders were compacted to pellets and electrodes to test the electrical and electrochemical properties, respectively. After pure LMnP and its doped versions were analyzed, it is understood that Co and V enhances the electrical and ionic conductivity of LMnP; whereas, Cr has a positive influence on the rate capability of LMnP.

To conclude, purity and particle size of LMnP are crucial for good electrochemical performance. The smaller the particle size of powders, the better the electrochemical performance. Furthermore, it is confirmed that Mn-site doping with Co, V and Cr enhances the conductivity and cycleability of LMnP.

APPENDIX

(a) GLU

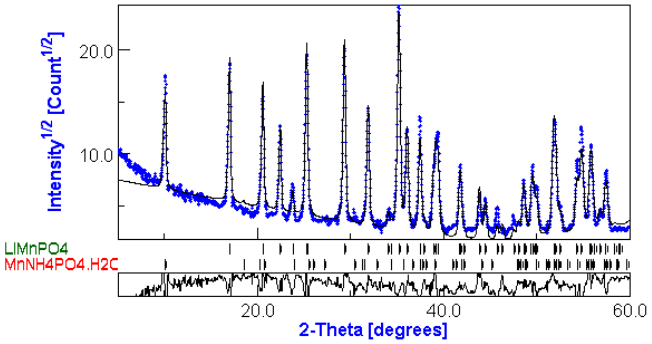

(b) CA

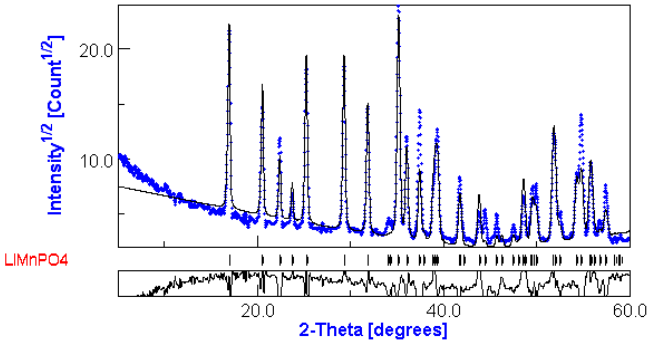

(c) EG

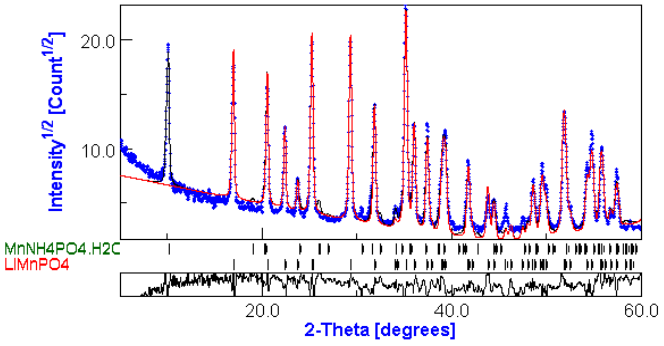

Figure 7.1. XRD patterns of the samples synthesized with additives.

(d) CTAB

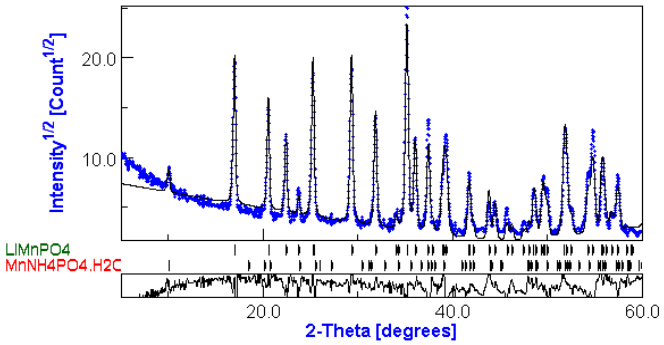

(e) SDS

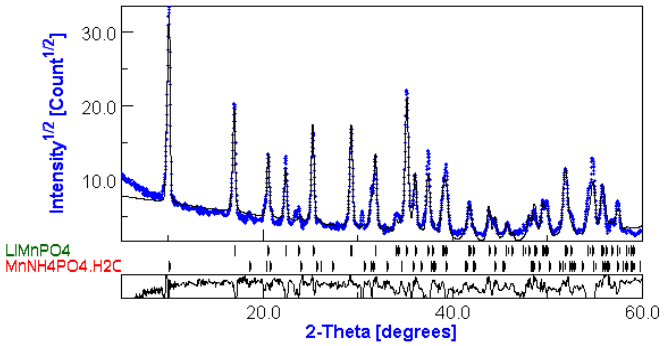

(f) PEG

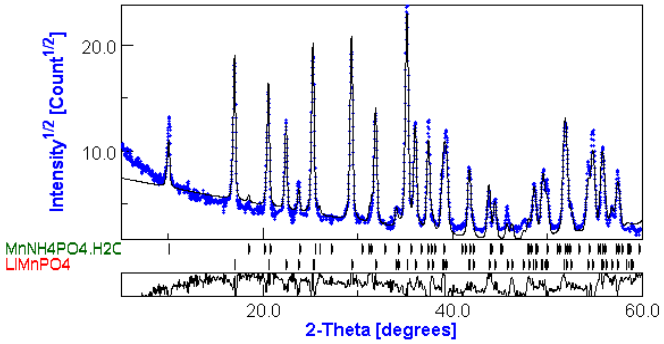

(g) PVA

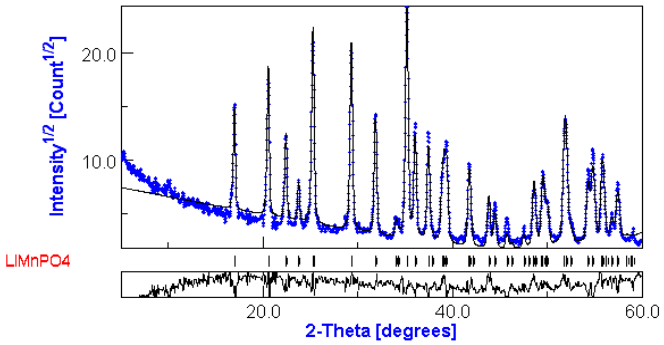

Figure 7.1. (Continued)

(h) IGE

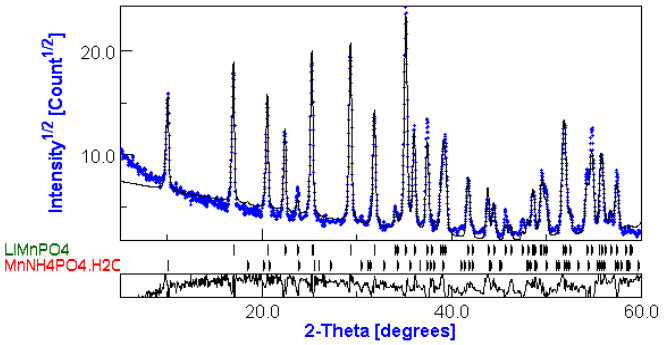

(i) GEL

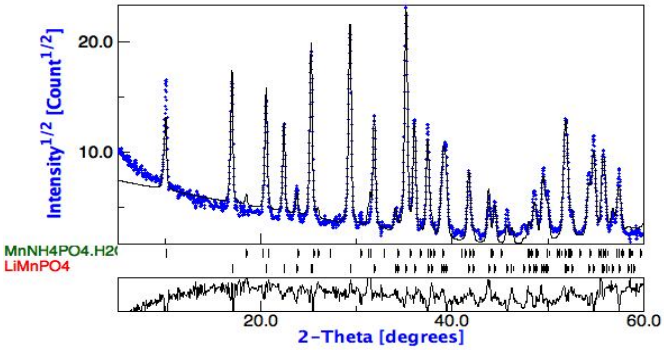

(j) LA

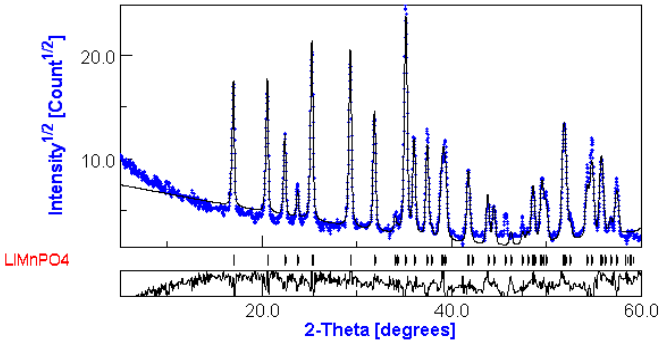

Figure 7.1. (Continued)

(a)

Co

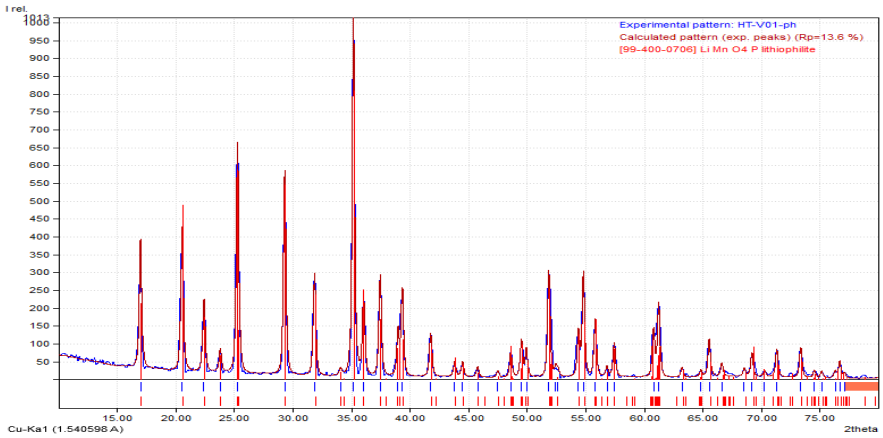

(b)

Cr

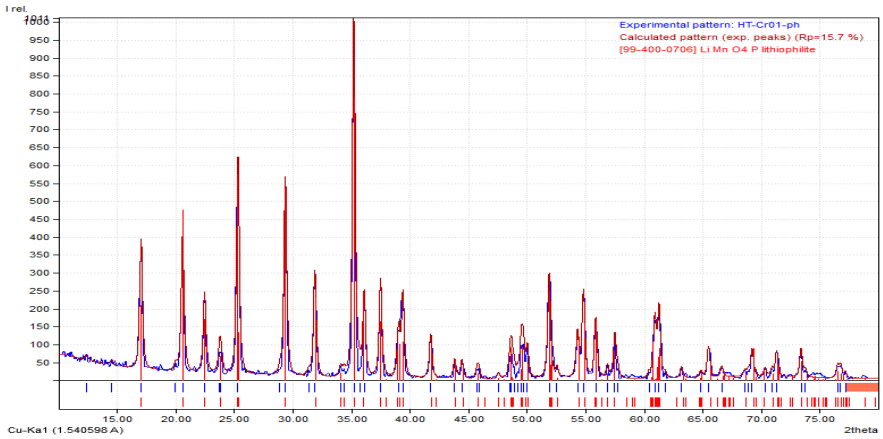

(c)

Mo

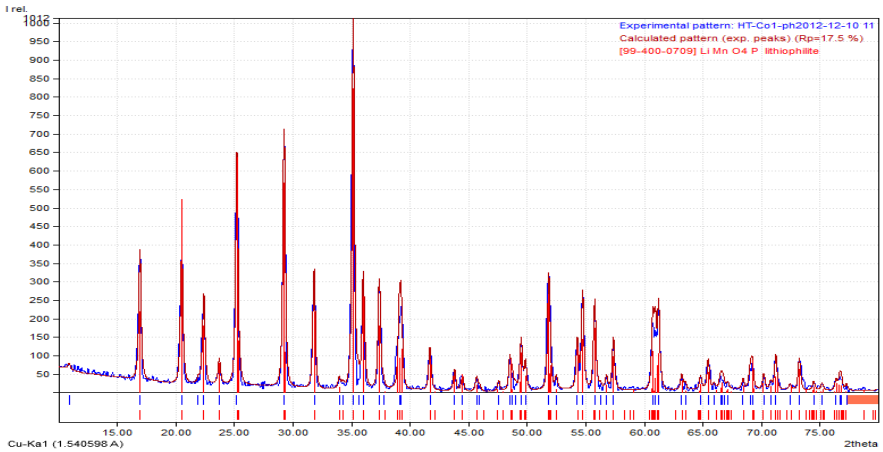

Figure 7.2. XRD patterns of the doped samples.

(d)

V

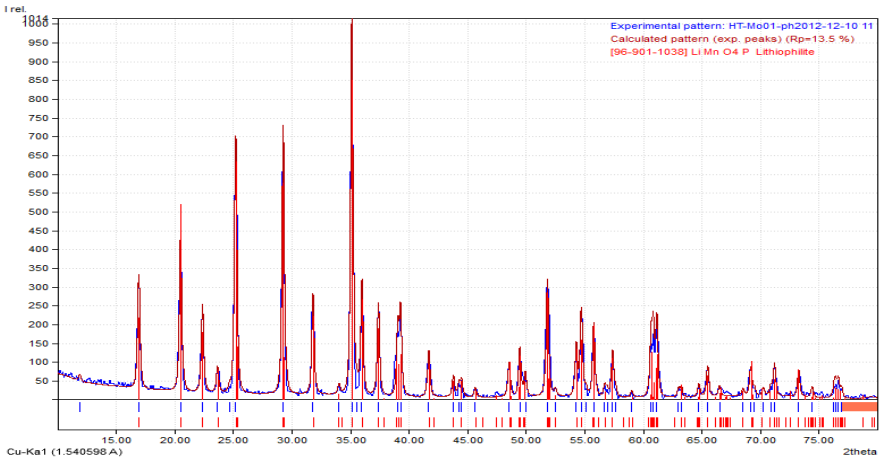

(e)

W

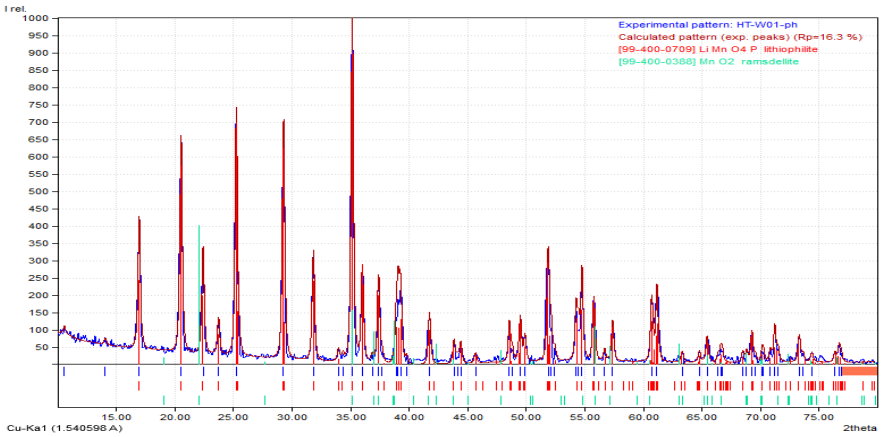

Figure 7.2 (Continued)

REFERENCES

[1] Zu, C.X. and H. Li, *Thermodynamic analysis on energy densities of batteries.* Energy and Environment Science, 2011. **4**(8): p. 2614-2620.

[2] Reddy, T.B., *Linden's Handbook of Batteries.* 4th ed. 2010.

[3] Root, M., *The TAB Battery Book.* 1st ed. 2010.

[4] Fletcher, S., *Bottled Lightning: Superbatteries, Electric Cars, and the New Lithium Economy*. 1st ed. 2011.

[5] Whittingham, M.S., *Electrical energy storage and intercalation chemistry.* Science,1976. **192**(6): p. 1126-1127.

[6] Mizushima, K. and J.B. Goodenough, *A new cathode material for batteries of high energy density.* Materials Research. Bulletin, 1980. **15**(7): p. 783-789.

[7] Yazami, R. and P. Touzain, *A reversible graphite-lithium negative electrode for electrochemical generators*. Journal of Power Sources, 1983. **9**(1): p. 365–371.

[8] Thackeray, M.M., W.I.F. David, P.G. Bruce and J.B. Goodenough, *Lithium insertion into manganese spinels*. Materials Research Bulletin,1983. **18**(8): p. 461-472.

[9] Padhi, A.K., *Phospho-olivines as positive electrode materials for rechargeable lithium batteries.* Journal of The Electrochemical Society, 1997. **144**(12): p. 1188-1197.

[10] Daniel, C. and J.O. Besenhard, *Handbook of Battery Materials.* 2nd ed. 2011.

[11] Whittingham, M.S., *Lithium batteries and cathode materials*. Chemical Reviews, 2004. **104**(4): p. 4271-4301.

[12] Besenhard, J.O., *Handbook of Battery Materials*. 1st ed. 1999.

[13] Oh, S.M., C.S. Yoon, B. Scrosati, K. Amine, and Y.K. Sun, *High-performance carbon-LiMnPO4 nanocomposite cathode for lithium batteries*. Advanced Functional Materials, 2010. **20**(19): p. 3260–3265.

[14] Blyr, A., *Self-discharge of LiMn2O4/C li-ion cells in their discharged state.* Journal of the Electrochemical Society, 1998. **145**(1): p. 194-201.

[15] Tarascon, J.M. and D. Guyomard, *The Li1+xMn2O4/C rocking-chair system: a review.* Electrochimica Acta, 1993. **38**(2): p. 1221–1231.

[16] Bakenov, Z. and I. Taniguchi, *LiMnPO4 olivine as a cathode for lithium batteries*. Journal of The Electrochemical Society, 2011. **75**(2): p. 222–227.

[17] Delacourt, C., L. Laffont, R. Bouchet, C. Wurm, J. Leriche, and M. Morcrette, *Toward understanding of electrical limitations (Electronic, ionic) in LiMPO4 (M = Fe, Mn) electrode materials*. Journal of The Electrochemical Society, 2005. **4**(2): p. 913–921.

[18] Yamada, A. and S. Chung, *Crystal chemistry of the olivine-type LiMnPO4*. Journal of The Electrochemical Society, 2001. **12**(5): p. 960–967.

[19] Yang, J. and J.J. Xu, *Synthesis and characterization of carbon-coated lithium transition metal phosphates LiMPO4 (M=Fe, Mn, Co, Ni) prepared via a Nonaqueous Sol-Gel Route*. Journal of The Electrochemical Society, 2006. **13**(5): p. 716-724.

[20] Murugan, A.V., T. Muraliganth and A. Manthiram, *One-pot microwave-hydrothermal synthesis and characterization of carbon-coated LiMPO4 (M=Mn, Fe, and Co) cathodes*. Journal of The Electrochemical Society, 2009. **156**(7). p. 79-87.

[21] Lee, J.W., M.S. Park, B. Anass, J.H. Park, M.S. Paik, and S.G. Doo, *Electrochemical lithiation and delithiation of LiMnPO4: Effect of cation substitution.* Electrochimica Acta, 2010. **55**(13): p. 4162–4169.

[22] Chung, S.Y., J.T. Bloking, and Y.M. Chiang, *Electronically conductive phospho-olivines as lithium storage electrodes*. Nature Materials, 2002. **1**(2): p. 123–128.

[23] Myung, S.T., S. Komaba, N. Hirosaki, H. Yashiro and N. Kumagai, *Emulsion drying synthesis of olivine LiFePO4/C composite and its electrochemical properties as lithium intercalation material*. Electrochimica Acta, 2004. **49**(24): p. 4213–4222.

[24] Matsuda, K. and I. Taniguchi, *Relationship between the electrochemical and particle properties of LiMn2O4 prepared by ultrasonic spray pyrolysis.* Journal of Power Sources*, 2004.* **132**(10): p. 156–160.

[25] Delacourt, C., P. Poizot, M. Morcrette, J. Tarascon and C. Masquelier, *One-step low-temperature route for the preparation of electrochemically active LiMnPO4 powders.* Journel of Power Sources, 2004. **5**(10): p. 93–99.

[26] Chen, J., S. Wang and M.S. Whittingham, *Hydrothermal synthesis of cathode materials*. Journel of Power Sources, 2007. **174**(2): p. 442–448.

[27] Moon, S., P. Muralidharan and D.K. Kim, *Carbon coating by high-energy milling and electrochemical properties of LiMnPO4 obtained in polyol process.* Ceramics International, 2012. **38**(20): p. 471–475.

[28] Chen, J., M.J. Vacchio, S. Wang, N. Chernova, P.Y. Zavalij and M.S. Whittingham, *The hydrothermal synthesis and characterization of olivines and related compounds for electrochemical applications*. Journal of The Electrochemical Society, 2008. **178**(14): p. 1676–1693.

[29] Chen, G.J., D. Wilcox and T.J. Richardson, *Improving the performance of lithium manganese phosphate through divalent cation substitution.* Journal of The Electrochemical Society, 2008. **48**(23): p. 190–194.

[30] Bramnik, N.N. and H. Ehrenberg, *Precursor- based synthesis and electrochemical performance of LiMnPO4.* Journel of Alloys and Compounds, 2008. **464**(14): p. 259–264.